



## Tuning mechanical properties of 3D printed composites with PLA:TPU programmable filaments



Aryabhat Darnal<sup>a</sup>, Zaryab Shahid<sup>a</sup>, Himani Deshpande<sup>b</sup>, Jeeeun Kim<sup>b</sup>, Anastasia Muliana<sup>a,\*</sup>

<sup>a</sup> Department of Mechanical Engineering, Texas A&M University, College Station, TX 77840, USA

<sup>b</sup> Department of Computer Science and Engineering, Texas A&M University, College Station, TX 77840, USA

### ARTICLE INFO

**Keywords:**

3D printing  
Programmable filaments  
PLA and TPU polymers  
Composites  
Tunable mechanical properties

### ABSTRACT

Polylactic acid (PLA) filament is widely used for desktop 3D printing purposes due to its exceptional mechanical properties such as high strength; however, its brittleness restricts its use for producing flexible objects. Thermoplastic polyurethane (TPU) filament which is also widely used for desktop 3D printing, on the other hand, is flexible and commonly used in printing compliant objects with relatively low load-bearing performance. This study investigates the ability to tune the mechanical properties of specimens that are printed using programmable filaments composed of PLA and TPU filaments with different volume ratios of PLA and TPU. Two types of PLA and TPU filament arrangements, i.e., series and parallel, are considered. The PLA:TPU programmable filaments are used to print dogbone specimens for tensile testing. In printing the dogbone specimens, the raster angle is varied, i.e., 0, 45, and 90° with respect to the transverse direction of the specimen. To examine their mechanical behaviors based on different PLA and TPU filament arrangements, compositions, and raster angles, tensile tests are conducted on both programmable filaments and dogbone specimens. This study demonstrates the ability to tune the mechanical properties of printed objects by designing programmable filaments and varying raster angles during printing.

### 1. Introduction

One of the most commonly used 3D printing techniques is Fused Deposition Modelling (FDM) or Fused Filament Fabrication (FFF) in which a thermoplastic filament as a source material is heated to its glass transition temperature,  $T_g$ , and extruded through the nozzle of the 3D printer for fabricating the desired object in a layer-by-layer fashion [1]. Polymers are used as the source material for FDM 3D printing. Several examples are Polylactic Acid (PLA), Polyethylene Terephthalate Glycol (PETG), Acrylonitrile Butadiene Styrene (ABS), Polyetheretherketone (PEEK), Thermoplastic Polyurethane (TPU), etc. Traditionally, FDM 3D printers were developed to use a single source filament [2]. This limits the mechanical properties and functionality of the 3D printable objects using FDM, because of the limited choice of filament materials that can be printed at a time. Multi-material 3D printing (MM3DP) leveraging either single or multi-extruders provides the opportunity to improve the performance of the fabricated part by varying material types and their compositions within the layers or the part which is not feasible using conventional FDM 3D printing with a single extruder [3]. Thus, material properties can be spatially varied to provide the desired properties in

specified locations of the object. Some applications of MM3DP include printing 3D circuits and all-printed resistor circuits, antenna, and metamaterials with enhanced dielectric and magnetic properties, high-performance biomedical implants, etc. [3]. The advantages of MM3DP are [3]:

- 1) It allows controlling material properties in a single fabricated part to increase the functionality of the products.
- 2) As the part can be fabricated in one build, it eliminates the need for component assembly, thereby reducing production costs and time.
- 3) It can lead to an integrated manufacturing system of complex structures.

Despite some advantages, MM3PD has some limitations, which are:

- 1) It requires post-processing (e.g. curing, sintering, annealing, removing chemical soluble support material) of the printed objects [4].

\* Corresponding author.

E-mail address: [amuliana@tamu.edu](mailto:amuliana@tamu.edu) (A. Muliana).

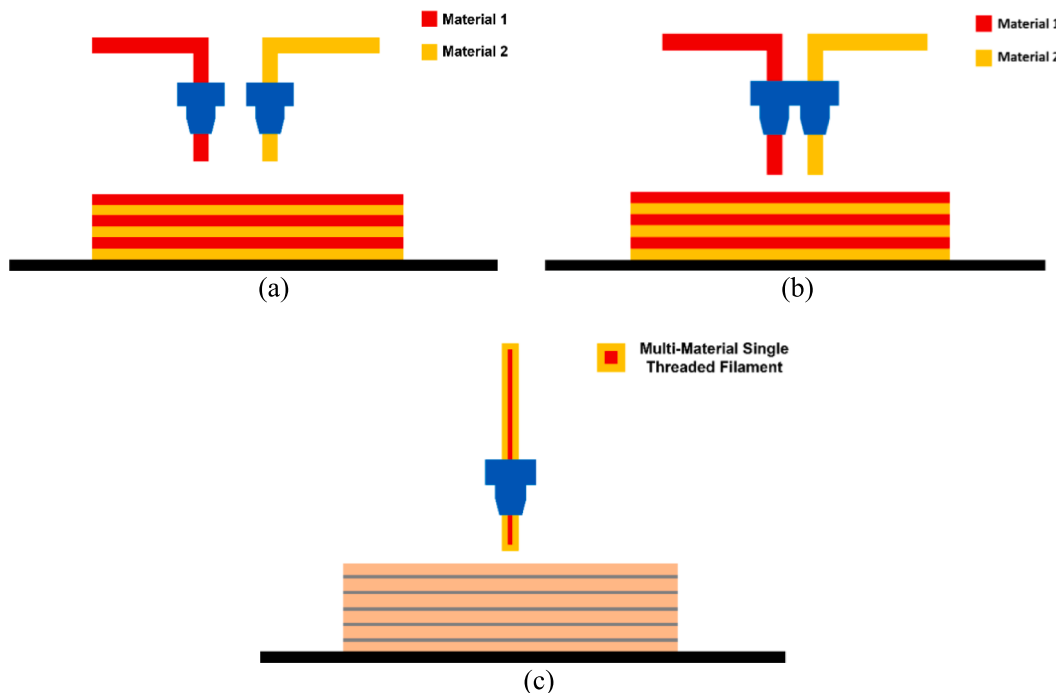


**Fig. 1.** (a) Multiple independent extruder nozzles; (b) Single head multiple extruder nozzles; (c) Single extruder nozzle with the multi-material single threaded filament for MM3DP.

- 2) It can develop weak interfaces in the layers of different materials due to the different thermal behaviors (thermal expansion, cooling rates, etc.) of the different materials [4].
- 3) In some cases, if a single extruder is used to print multiple materials, it causes process interruptions, residual materials trapped in the nozzle during switching, and loss of time due to material changeover and removing residual materials [3].

The existing studies suggest several ways of MM3PD: using two or multiple extrusion heads each for different material [3,5–11] and using a single multi-material filament as a feedstock similar to using a single material thermoplastic filament [12–15], as illustrated in Fig. 1.

Dual or multiple extruder printing heads are the most common approach to printing multiple materials [5], see Fig. 1a. Zhou et al. [16] designed and constructed a novel single-screw extrusion-based printing system by modifying a Touch 3D FDM machine allowing the mixing and printing of multiple materials to fabricate 3D objects. It contains a rotating screw inside a heated barrel with multiple openings which is used for feeding multiple materials. The technology has the potential to print objects with controllable and variable properties. Khondoker et al. [6] built a custom bi-extruder FDM system designed to use 3-mm diameter filaments to print functionally gradient materials made up of immiscible polymers. Their FDM allows the printing of two dissimilar thermoplastic materials with side-by-side extrusion and mechanically interlocked extrusion, reducing adhesion failure between filaments. Voxelated soft matter (designed and fabricated in voxel-by-voxel) was achieved using a multi-material multi-nozzle 3D printer (MM3D) [8]. Multiple filament materials are switched and used at high frequencies in the MM3D printer head enabling continuous printing of heterogeneous voxelated filaments. These filaments are then used to rapidly construct objects with spatially designed compositions and properties. Kwon et al. [17] proposed modifying the interface geometry by modifying the G-code and printing parameters to print multiple materials (PLA, TPU, ABS, PETG) with enhanced interlocking structures to achieve improved adhesion between dissimilar materials in FDM.

For using a single multi-material filament (Fig. 1c), Hart et al. [13] fabricated novel dual-material (DM) filaments comprising two

thermoplastic filaments Acrylonitrile Butadiene Styrene (ABS) and Polycarbonate (PC) which differ in their glass transition temperature ( $T_g$ ) by 36 °C via thermal drawing preform. These DM filaments were then used as feedstock for making 3D objects with ABS and PC with various microstructures. These 3D-printed objects are then subjected to annealing temperatures between the  $T_g$  of ABS and PC resulting in superior fracture toughness which is otherwise not achievable using either of these materials. Tao et al. [12] demonstrated the compatibility of TPU/PLA composite filament with the FDM 3D printing process. These filaments are fabricated by blending pellets of PLA and TPU with different ratios of TPU/PLA (0/100%, 25/75%, and 50/50% by weight). These composite filaments are then used to 3D print dogbone specimens. Loke et al. [14] constructed filaments with different interchangeable materials with predefined interfaces using an external adhesion promoter and fed them into a regular FFF printer with a modified nozzle for 3D printing of optoelectronics. Kalita et al. [15] fabricated a composite filament made up of Tricalcium Phosphate (TCP) and Polypropylene (PP). The compounded mixture of TCP and PP is manually grounded into small pellets and extruded into filaments with 1.78 mm diameter.

From the existing methods for multi-material FDM 3D printing discussed above, the major limitations are highlighted below:

1. They require hardware upgrades, e.g., multiple printer heads, one head with multiple feeders, and customization of currently available FDM 3D printers.
2. They often require pre and post-processing methods (dehydrating thermoplastic pellets, heat treatments) to either fabricate the filaments or the composite objects.
3. These methods do not control the spatial configuration of the materials in the multi-material filament, making it difficult to tune the properties of the 3D-printed object.
4. Printing a single-threaded, multi-segmented filament still requires manually exchanging the resource filaments when switching the color and/or material, which is very time consuming [18] and labor intensive [17].

To overcome the above limitations, we propose using the

programmable filament technique, which has been initially explored by Takahashi et al. [18] to print objects with multiple colors using a regular FDM 3D printer requiring no hardware updates. The idea is to enable the printing of multi-material objects using a low-cost FDM printer without requiring any hardware updates. The technique involves connecting segments of two or more materials into a single filament based on the required specifications (the configuration, arrangement, and composition) to fabricate a single object possessing new material properties, previously unseen in single materials. This approach also helps in cutting production costs and time [2]. In this paper, we investigate the mechanical properties of the 3D-printed programmable filaments made from a combination of PLA and TPU as they are commercially available for FDM 3D printing, presenting significantly different mechanical properties. In this study, the programmable filaments with different PLA:TPU volume ratios and two arrangements of PLA and TPU, which are series and parallel, are first printed. These filaments are tested under uniaxial tension to first examine their mechanical behaviors. Dogbone tensile specimens are then printed out of some of these programmable filaments. Different raster angles, i.e., 0, 90, and 45°, with respect to the transverse direction of the specimen are considered to examine the possible anisotropic mechanical responses of materials. Uniaxial tensile tests are performed on the dogbone specimens to examine the influence of layer arrangements (series and parallel) and PLA:TPU compositions of the programmable filament and raster angles on the mechanical properties of the printed specimens. This paper is organized as follows. **Section 2** discusses processes and parameters for programmable filament printing. **Section 3** presents the printing process for PLA:TPU filaments and dogbone specimens using programmable filaments produced in **Section 2**. **Section 4** discusses testing the mechanical properties of the programmable filaments and dogbone specimens, followed by the results in **Section 5**. **Section 6** is dedicated to the discussion and conclusion.

## 2. Programmable filament

The concept of programmable filaments was used to 3D print objects with multiple colors using a single header FDM 3D printer as explored and discussed in detail in [18]. Multiple segments of different thermoplastic filaments are connected and fabricated into a single filament which is then treated as a single material filament and fed into the 3D printer. The name “programmable” filament signifies that the material properties of the printed object can be tuned based on the composition, configuration, or processing parameters of the printing process. This technique can potentially produce new material properties that are not seen in typical or available thermoplastic filaments. Takahashi et al. [18] demonstrated that these filaments can be used similarly to a conventional thermoplastic filament, which is extruded through a standard nozzle of an FDM 3D printer. Although this method still requires the manual change of the source filament when switching between materials when constructing a filament, the number of manual changes is still lower than what is required for traditional printing using a single extruder printer, and no need for the material change needed when printing a 3D object using programmable filament [18].

The procedure of printing a single-threaded two-material programmable filament (series configuration) is illustrated in Fig. 2. First, the extruder of the printer moves around the printing bed (red) depositing the first material (grey) in a spiral pattern mimicking a filament spool as the first layer, without any sharp turns ensuring the final printed filament can be easily fed into the extruder (see Fig. 2a). In the rest of the layers, depending on the selected configuration and constituent compositions in the programmable filament, the extruder leaves gaps that will later be filled with the second material (i.e., series configuration, see Fig. 2b). The parts of the printed filament where the first material is deposited are geometrically set through the G-code script. Once the extruder has finished depositing the first material, the printing is paused and the filament needs to be manually changed to the second material.

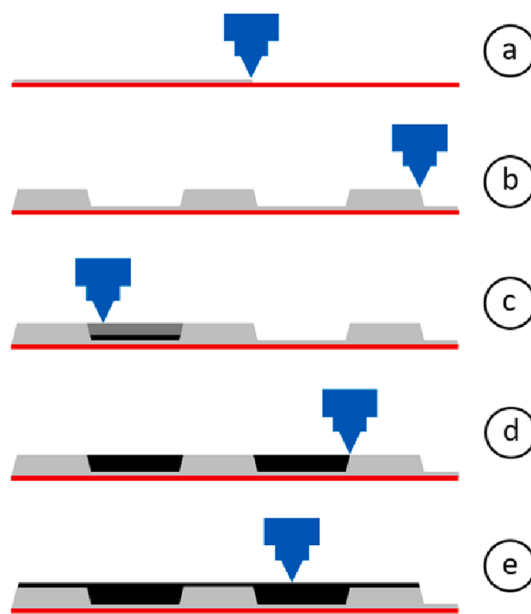


**Fig. 2.** (a-b) Extruder prints a complete layer with the first material. (c-d) The second material fills in the gaps/areas of the already printed filament to complete the filament shape. (e) One last layer of the second material is printed over the entire filament to ensure the adhesion of both the material sections in the printed filament.

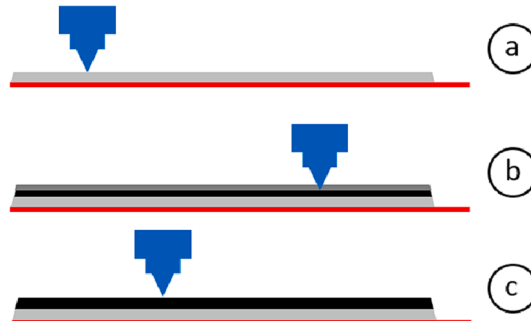


**Fig. 3.** (a) Extruder first prints a complete layer with the first material. (b-c) The second material is deposited on top of the first material completing the printed filament.

On resuming the print, the extruder then fills in the parts of the printed filament that are programmed to be in the second material (black), see Fig. 2c and d. One last layer of the second material is printed over the entire filament to ensure the adhesion of both the material sections in the printed filament (Fig. 2e). As can be seen from Fig. 2, for the series configuration, the deposited materials form an interlocking structure enabling easy deposition without extruder-material interference during the printing time.

In the case of the parallel configuration, the extruder of the printer moves around the printing bed (red) depositing the first material (grey) in a spiral pattern mimicking a filament spool as the first layer, (see Fig. 3a). Then, the second material is simply deposited on top of the first material completing the printed filament, see Fig. 3b and c.

The programmable filaments are intended for a cylindrical shape of a circular cross-section of a certain diameter; however, from the printing process, we cannot get a perfectly circular cross-section (see **Section 3**). The first layer conforms to only one or two strokes, the second layer conforms to two to three strokes, and so on. Gradually varying the stroke counts was considered to form a nearly circular shape of the programmable filament cross-section.

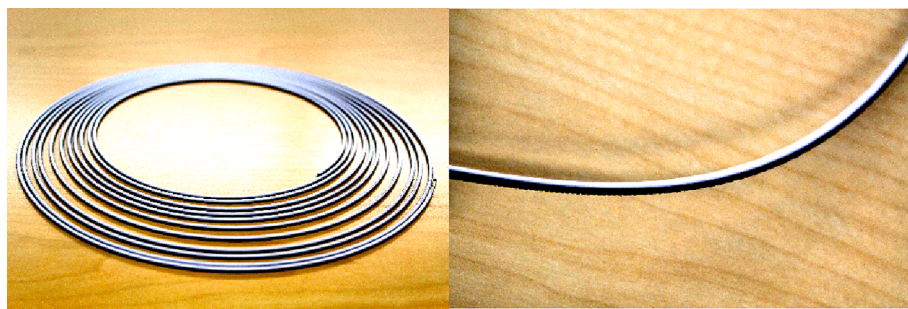


**Fig. 4.** Programmable Filament with a parallel configuration of PLA (black) and TPU (white).



**Fig. 5.** Programmable Filament with a series configuration of PLA (black) and TPU (white).

**Table 1**  
Printing Parameters.

Parameter	Unit	Programmable filament	Dogbone specimen
Print Temperature	°C	220	220
Bed/Surface Temperature	°C	60	60
Print Speed	mm/s	40	40
Layer (Shell) Thickness	mm	0.25	0.25
Flow Rate	%	100	100
Infill Density	%	–	100
Bed Adhesion	N/A	Brim	None

**Table 2**  
Diameters of the filaments used for tensile testing.

Type	Material(s)	Diameter (mm)
		Avg. ± S.D.
Parallel	Unprinted PLA	1.747 ± 0.019
	Printed PLA	1.5 ± 0.019
	PLA:TPU = 70:30	1.59 ± 0.062
	PLA:TPU = 60:40	1.52 ± 0.029
Series	PLA:TPU = 50:50	1.66 ± 0.072
	PLA:TPU = 40:60	1.62 ± 0.032
	PLA:TPU = 70:30	1.59 ± 0.084
	PLA:TPU = 60:40	1.61 ± 0.033
	PLA:TPU = 50:50	1.59 ± 0.026
	PLA:TPU = 40:60	1.58 ± 0.096
	Printed TPU	1.51 ± 0.065
	Unprinted TPU	1.747 ± 0.019

### 3. Materials and printing process

The PLA and TPU filaments used in this study are manufactured by Overture 3D. Both filaments have an outer diameter of 1.75 mm. PLA possesses relatively high strength and rigidity, great optical properties [19], excellent manufacturing capability, and is biocompatible and biodegradable, which is suitable for biomedical devices (surgical sutures, bone screws, bone plates, etc. [20]). However, PLA is relatively brittle, which can limit its applications. According to Oksiuta et al. [19],

the total elongation under a tensile load is approximately 3% and the toughness is relatively low. To enhance its ductility Jaso et al. [20] combined PLA with polyethylene, synthetic rubbers, starch, poly (butylene succinate), poly (hydroxy alkanoates), polymerized soybean oil, and polyamide. However, the composites had limited success due to the reduced biocompatibility and biodegradability. Several studies [12,20–22] have shown that TPU is an ideal material that can be combined with PLA resulting in improved flexibility of the system. TPU is a thermoplastic elastomer characterized by high toughness, low elastic modulus, and biocompatibility. TPU elastomer is composed of soft and hard segments. The soft segments consist of polyester or polyether, which is miscible PLA [23]. The carbamate from hard segments of TPU can form hydrogen bonds with PLA [23]. Both PLA and TPU have ester bonds in their main polymer chains [20]. The above properties make TPU compatible with PLA.

We investigate programmable filaments containing PLA:TPU in different volume ratios of 40:60, 50:50, 60:40, and 70:30 by extruding them through a single extruder with two configurations, as shown in Figs. 4 and 5. A lower ratio of PLA was not considered as we want to maintain relatively high strength with is attributed to the PLA. The printing parameters (Table 1) used for printing the filaments are selected for the following reasons:

- The recommended nozzle/print temperature for PLA filament by the manufacturer is 190 – 220 °C and TPU filament is 210 – 230 °C (Overture 3D). A higher nozzle temperature leads to better layer adhesion, therefore 220 °C is selected as the nozzle/print temperature.
- The recommended bed/surface temperature for both PLA and TPU filament is 25 – 60 °C (Overture 3D). Higher bed temperature leads to reduced surface tension between the bed and deposited material and a larger contact area, leading to better adhesion between the filament and bed [24] and reducing temperature gradients between the recent and previously printed layers that cause warping. A bed temperature of 60 °C is selected.
- The recommended printing speed for PLA filament is 40 – 90 mm/s and TPU filament is 20 – 40 mm/s (Overture 3D). The printing speed of 40 mm/s is selected as it agrees with the recommended range for both filament materials, requiring no changes in settings.

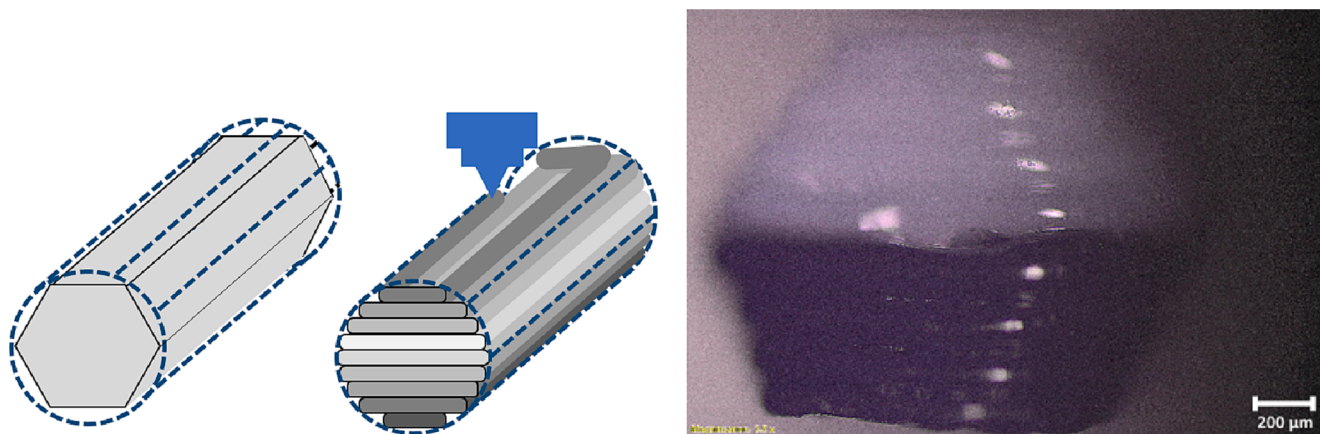


**Fig. 6.** Left: A schematic of a cross-section of a programmable filament. Right: Parallel Programmable Filament of PLA:TPU = 50:50 (the top is TPU and the bottom is PLA).

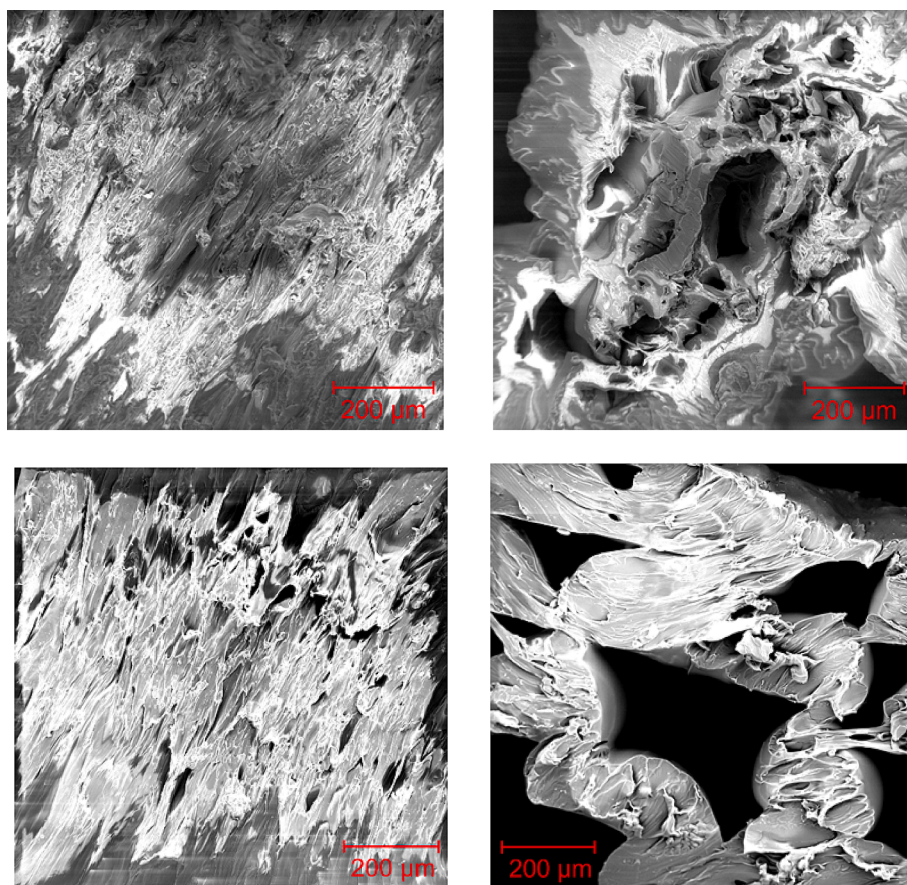
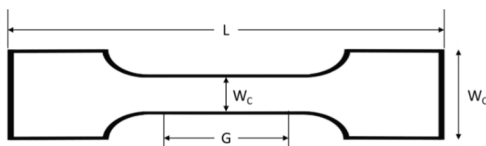


**Fig. 7.** Unprinted (top left) and printed (top right) PLA filament and unprinted (bottom left) and printed (bottom right) TPU filament.



Gage Length (G) =  $25.59 \pm 0.39$  mm      Overall Length (L) =  $114.04 \pm 0.661$  mm  
 $3.77 \pm 0.021$  mm

**Fig. 8.** Dimensions of the 3D-printed dogbone specimen,

- d) The single-threaded programmable filament is a solid volume, therefore a flow rate of 100% is selected. The 3D printer's default layer thickness is 0.2 mm for the 0.4 mm nozzle diameter. We found that 0.25 mm layer thickness has no significant printing quality differences but it reduces the printing time as fewer printing layers are needed.

We also investigate the effect of the 3D printing process on the PLA and TPU filaments by extruding/printing single filaments using the same process parameters given in Table 1. The original PLA and TPU filaments have a 1.75 mm diameter, and for the programmable filaments as well as the printed PLA and TPU filaments, there are variations in the diameter, ranging from 1.5 mm to less than 1.7 mm, as reported in Table 2. It is

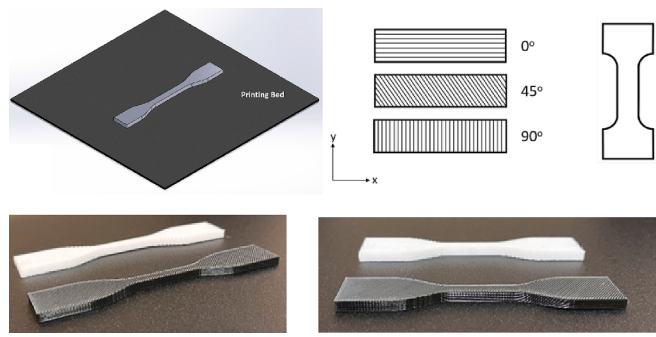


**Fig. 9.** Top: Flat Build orientation for printing of the dogbone samples (left) and raster angles with respect to the transverse direction of the dogbone specimen (Note: 0° raster angle is parallel to the x-axis. 90° raster angle is perpendicular to the x-axis.) Bottom: Examples of printed dogbone specimens.



**Fig. 10.** Dogbone specimens (PLA – PLA:TPU 40:60 Parallel – PLA:TPU 40:60 Series – TPU) with raster angles 0° (top), 45° (middle), and 90° (bottom).

noted that the printing process drastically reduced the diameter of the filaments. The extruded single filament shows less than 200  $\mu\text{m}$  (approximately) and multiple layers are printed to achieve an overall diameter between 1.5 mm and 1.7 mm. Also, for the printed filaments and programmable filaments, the cross-section is not perfectly circular,

but rather of a polygon shape. **Fig. 6** illustrates an example of the cross-section of a programmable filament of PLA:TPU = 50:50 with a parallel arrangement.

We also report the scanning electron microscopy (SEM) images highlighting the differences in the microstructures of unprinted and printed filaments for both PLA and TPU, shown in **Fig. 7**. A significant shrinkage in the filaments after passing through the extruder is seen. This shrinkage causes densification of the filament, which can affect the stiffness of the printed filament. To form printed PLA and TPU filaments that can be tested, multiple layers of extruded filaments are considered as discussed in **Section 2**, see an example in **Fig. 6**. Porosity is formed in the printed filaments, which can affect their mechanical properties, which is discussed in the experimental results (**Section 5**).

We then print dogbone specimens out of some of these programmable filaments to examine the tensile mechanical properties of printed objects using the programmable filaments. The dogbone specimens are designed based on ASTM D638-14 Type IV standards [25]. The shape and dimension of the dogbone specimen (with average and standard deviation) are shown in **Fig. 8**. The dogbone specimens are sliced using Ultimaker CURA open-source slicer (Ver. 4.9.1) and printed using a single header Ender 3 FDM 3D printer, with a nozzle of 0.4 mm diameter, a heated bed system. The printing parameters for fabricating the dogbone samples are presented in **Table 1**. The infill density to print the dogbone specimens is chosen due to printing with solid filaments.

The dogbone specimens are printed with a flat build orientation (see **Fig. 9 top left**). Different raster angles: 0°, 45° and 90° are considered during the dogbone printing. Dogbone specimens out of pure PLA and pure TPU are also printed with different raster angles for comparison. **Fig. 9 top right** shows the pattern of the filament deposition for each layer for each of the raster angles. The 3D printed specimens are modeled using SolidWorks software and exported as an STL file and imported to the 3D printing software. No thermal distortions or warping are seen in the printed samples, see examples in **Fig. 9 bottom**. Examples of the printed dogbone specimens are shown in **Fig. 10**. The dogbone specimens in **Fig. 10** are printed using the programmable filaments having a PLA:TPU = 40:60. It is seen that the use of programmable filaments generates a relatively uniform material distribution in the printed dogbone specimens.

Examples of SEM images of the printed dogbone specimens are shown in **Fig. 11**. The pure TPU printed specimens have much more porosity compared to the rest of the printed specimens. The alternating regions with PLA and TPU materials can be seen clearly in the specimens with parallel arrangements of the programmable filaments. For the specimens printed with series arrangements of the programmable filaments, a more complex pattern of PLA and TPU materials is observed. These microstructural characteristics can have a pronounced impact on the mechanical properties of the printed specimens, which will be discussed in **Section 5**.

#### 4. Experimental test

This section discusses the uniaxial tensile tests to evaluate the mechanical properties of the programmable filaments (both series and parallel configurations) and dogbone specimens printed out of the programmable filaments. The mechanical properties of PLA and TPU filaments and dogbone specimens printed out of PLA and TPU filaments are also evaluated for comparisons.

All six categories of filaments (Unprinted PLA, Unprinted TPU, Printed PLA, Printed TPU, parallel programmable filaments in varying PLA:TPU volume ratio, and series programmable filaments in varying PLA:TPU volume ratio) are subjected to tensile force in an Instron 5984 Floor Standing Universal Testing Machine using displacement control. Cord capstan grips which are designed to test cord specimens were used. We follow the ASTM D2256 standard for testing continuous filament. The diameter of the filaments is measured at three different locations between the grips of the cord capstan grips. The average and standard

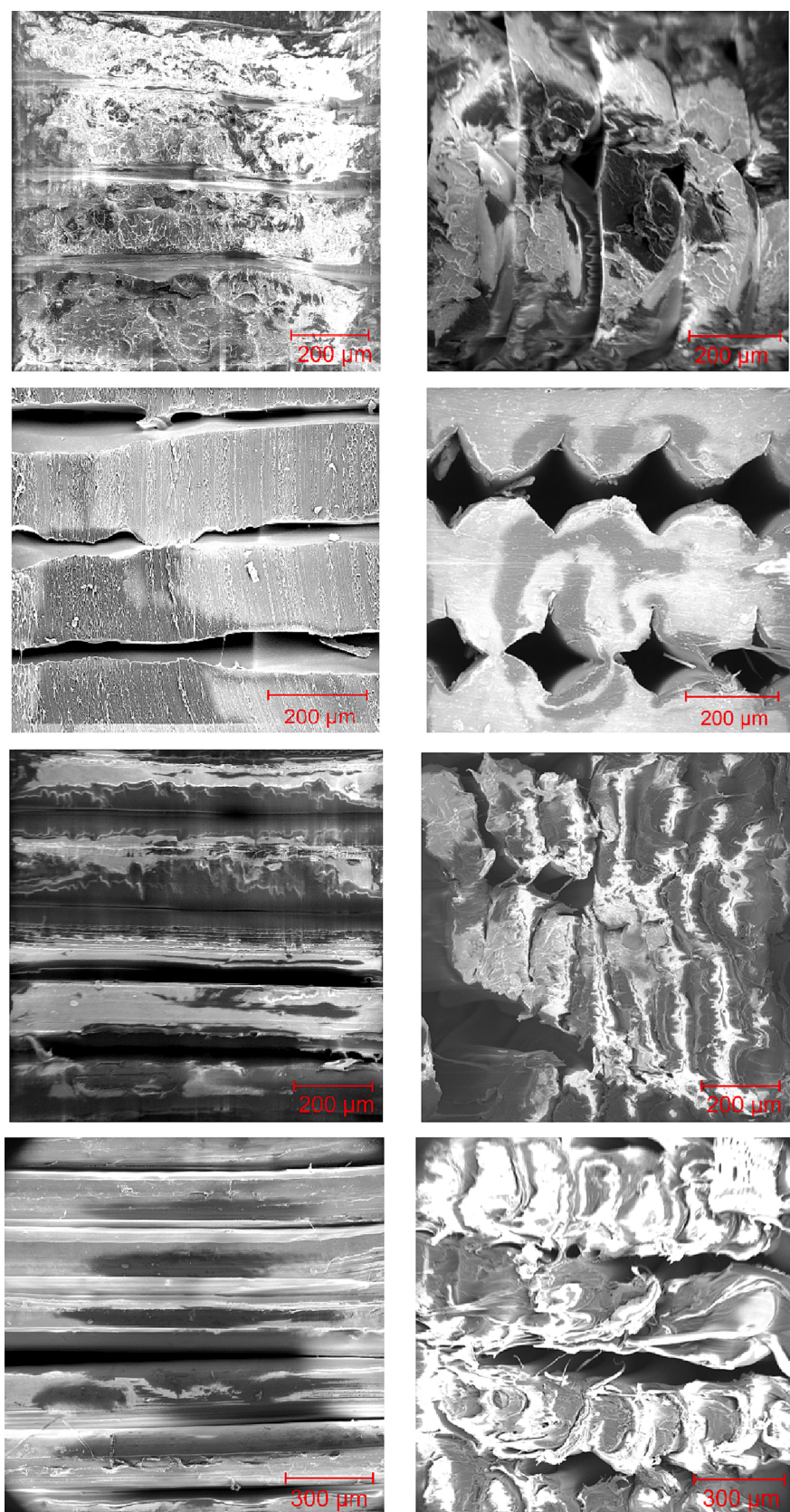


**Fig. 11.** SEM images of printed dogbone specimens with raster angles 0° (left) and 90° (right). Top to bottom: PLA, TPU, PLA:TPU 40:60 Parallel – PLA:TPU 40:60 Series (a higher resolution for the last images is needed for sharper images).



**Fig. 12.** Filament Tensile Testing using Cord Capstan Grips.

deviation in the measurement of the filament diameter is given in Table 2. The filament testing is illustrated in Fig. 12. The programmable filaments have different PLA:TPU volume ratios (40:60, 50:50, 60:40, 70:30). The tests were repeated 3 times for all types of filaments. All filaments were stretched with a displacement rate of 2 mm/sec. The corresponding stress-strain curves were recorded. The elastic modulus was determined from the slope of the stress-strain curve in the initial region. The tensile strength was chosen at which the tensile stress reaches its peak value just before failure starts occurring. The strain at failure was the last strain at which the filament lost stability.

For testing the dogbone samples, the ASTM D638-14 Type IV standard [25] was followed. The tests were conducted on Instron 5984 Floor Standing Universal Testing Machine with a 5kN load cell. A displacement rate of 1 mm/s was used in all specimens. The elastic modulus and tensile strength of the dogbone specimens were determined from the stress-strain curves similar to the ones of the filaments. As some dogbone specimens show a progressive degradation while others showed a sudden failure and lost stability, the failure strain was considered when the stress started to decrease from the peak stresses.

## 5. Results

The mechanical properties of the programmable filaments are first examined and compared to the responses of PLA and TPU filaments. In the next section, the mechanical properties of the 3D-printed dogbone specimens made of programmable filaments are investigated and their responses are compared to the ones printed using PLA and TPU filaments. For consistency in measurements, average strains, which are determined from the axial displacements, are used since characterizing local strains in the filaments using DIC or extensometer is unfeasible.

### 5.1. Mechanical behaviors of programmable filaments

The representative stress-strain curves for all the filaments are presented in Figs. 13–15. Printing changes the mechanical behaviors of the PLA and TPU filaments, as shown in Fig. 13. The printing process results in significantly brittle PLA filaments with reduced load-bearing ability, while only slight changes are seen in the TPU filaments. The elastic modulus of the printed PLA filaments increases by 267% as compared to

the unprinted PLA filaments, whereas the tensile strength and failure strain decrease by 38% and 71%, respectively. The changes in the stiffness and strength of the printed PLA filaments are likely because the filament densification from printing increases the stiffness while the porosity of the printed PLA can induce early failure (see Fig. 7). The insignificant changes in the mechanical properties of the TPU filaments are likely because of the very high porosity in the printed TPU filament which offset the filament stiffening from densification. The responses from the printed PLA and TPU filaments will be compared to the ones of programmable filaments.

The programmable filaments with series and parallel arrangements have different mechanical behaviors, which are also different than the behaviors of PLA and TPU filaments (Figs. 14 and 15). The responses from repeated tests, which show consistent responses, are given in the Appendix. The programmable filament with parallel arrangement can be tuned to control the strength and stiffness of the filament by varying the PLA:TPU ratios, while the failure strains of the programmable filaments remain close to 7%. As the percentage of PLA is decreased from 70% to 40%, the elastic modulus (stiffness) and strength of the programmable filaments with a parallel configuration decrease, as shown in Fig. 14.

The programmable filament with a series arrangement shows a softening mechanical response with failure strains ranging from 5% to 14%. The stiffness and strength of the programmable filaments in a series configuration are significantly lower than those of the programmable filaments in a parallel configuration. For both elastic modulus and strength, there is no clear trend as the ratio of PLA:TPU is changed, while the strain to failure increases with increasing the TPU ratio. Considering the consistency in the repeated tests and relatively low standard deviations (see Appendix) the random variations in the strength and stiffness at different PLA:TPU ratios are unlikely attributed to inconsistent printing and experimental errors.

The two programmable filaments exhibit different failure mechanisms (Fig. 16), which are attributed to the different microstructural patterns of the filaments (see Figs. 4 and 5). The series arrangement indicated that failure occurred at the interface of the PLA and TPU, and thus future studies on increasing the interface bonding can improve the load-bearing ability of this programmable filament. The parallel arrangement showed failure occurred by breaking the PLA filament due to its low strain to failure, which explains the similar strain to failure for all programmable filaments with parallel PLA:TPU arrangements.

The performance of the programmable filaments indicates the capability to create new material properties that are different from the properties of their parent filaments (PLA and TPU). The parallel arrangement can be used to tune the strength and stiffness, while the strain to failure can be tuned by a series arrangement. The mechanical properties of the thermoplastic filaments (PLA and TPU) and programmable filaments (parallel and series configuration) are characterized by the tensile test results. These include elastic modulus denoted by  $E$  (MPa), tensile strength denoted by  $\sigma$  (MPa), and strain at failure denoted by  $\epsilon_f$ . We also determine the margin of error (MOE) to examine the reliability of the experimental data (see Figs. A.3 and A.4 in the Appendix). A lower value of MOE indicates a higher reliability of the experimental data and that it can confidently represent the population of the specimens. According to studies [26–30], a MOE of less than 10% is considered for the reliability of the data. The MOE values for the tested filaments are less than 8%, except for the strain at failure for the PLA:TPU = 50:50 filament which is 13.8%. The result indicates the reliability of the experimental data. The mechanical properties for both parallel and series programmable filaments are summarized in Figs. 17 and 18. The average and standard deviation values of these properties are listed in Tables A.1 and A.2 in the Appendix.

### 5.2. Mechanical behaviors of dogbone specimens

The uniaxial tensile test results from the dogbone specimens printed

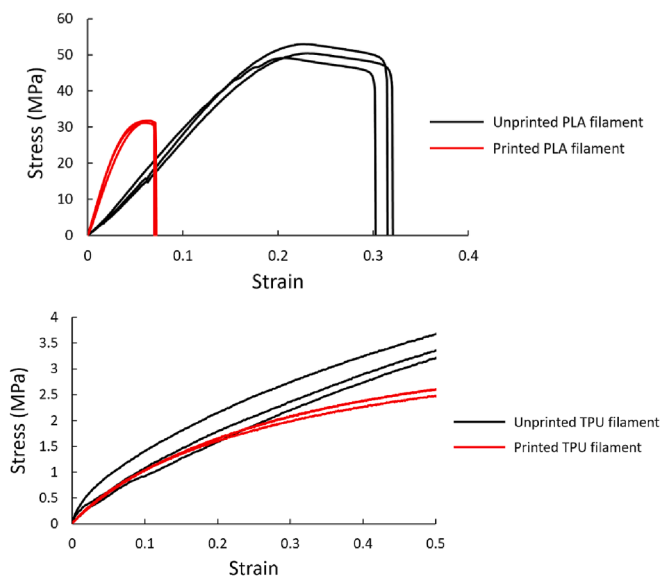


**Fig. 13.** Representative Stress-Strain curve for unprinted and printed PLA filament (top) and unprinted and printed TPU filament (bottom).

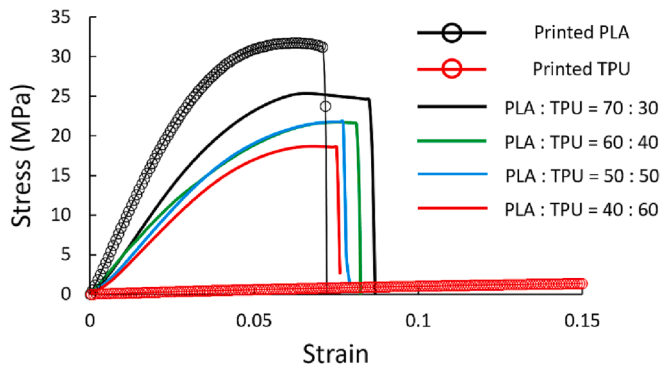


**Fig. 14.** Representative Stress-Strain curve for printed PLA filament, PLA:TPU programmable filaments with a parallel arrangement and printed TPU filament.

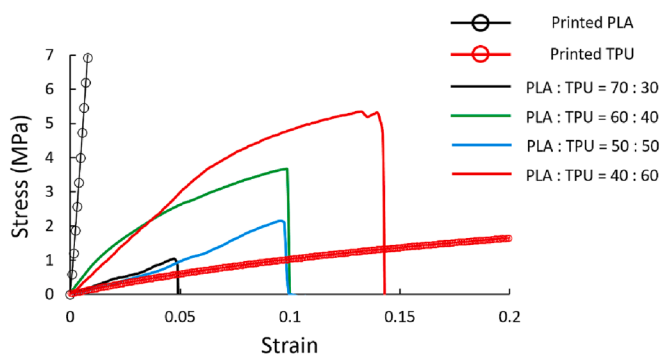


**Fig. 15.** Representative Stress-Strain curve for printed PLA filament, PLA:TPU programmable filaments with a series arrangement and printed TPU filament.

using PLA, TPU, and programmable filaments with series and parallel arrangements are shown in Fig. 19. These are the representative stress-strain curves for the dogbone specimens printed with different raster angles 0°, 45°, and 90°. For the dogbone specimens printed with programmable filaments of a series arrangement only PLA:TPU 40:60 ratio is used since this filament gives the highest strength. For the parallel arrangement, the PLA:TPU ratios of 60:40 and 40:60 are considered. The results from repeated tests can be found in Figs. A.5-A.9 in the Appendix. The overall elastic modulus, tensile strength, and strain to

failure are summarized in Tables A3-A5 in the Appendix.

For the PLA specimens, the responses from the different raster angles are relatively similar (Fig. A.5) with nearly the same values for the elastic modulus, tensile strength, and strain to failure, although there are slight changes in the failure mechanisms. The specimens printed with 0° and 45° raster angles failed due to printing layer separations, while the one printed with the 90° raster angle fails due to breakage perpendicular to the printing layers (see Fig. 20). For the TPU specimens, varying the raster angles significantly alters the mechanical properties of the printed specimens (Fig. A.9). Increasing the raster angles from 0°, 45°, to 90° increases the strength, stiffness, and failure strain. The failure mechanisms of the specimens for all raster angles are due to printing layer separations.

For all dogbone specimens printed with programmable filaments, their strength and stiffness are lower than the ones of PLA specimens and higher than the ones of TPU specimens, printed with the same raster angle. The dogbone specimens printed at a raster angle of 90° have the highest strength and stiffness when compared to the ones printed with 0° and 45° raster angles. The specimens printed with 0° and 45° raster angles failed due to printing layer separations, while the ones printed with 90° raster show much more complex failure patterns as the TPU layers tend to hold the samples together while the PLA layer breaks, which delays specimen failures (Fig. 20).

The average and standard deviation values of the mechanical properties of the printed dogbone specimens are summarized in Figs. 21-23. For the dogbone specimens printed with parallel programmable filaments, the elastic modulus and tensile strength of the specimens printed with PLA:TPU ratios of 60:40 and 40:60 are similar for the 0° raster angle. For the 45° and 90° raster angle specimens, the higher percentage of PLA leads to higher elastic modulus and tensile strength. This is consistent with the mechanical response of the parallel programmable filaments. For the specimens printed with series programmable filaments, for all raster angles, the specimens have a higher elastic modulus as compared to the ones printed with parallel programmable filaments. All the series programmable specimens present a higher tensile strength as compared to their parallel counterpart, which is interesting considering that the programmable filaments with a series arrangement are significantly weaker than the ones of a parallel configuration. In the dogbone specimens with series programmable filaments at a fixed PLA:TPU ratio, increasing the raster angles from 0°, 45°, and 90° increases the stiffness and strength. The failure strains in the dogbone specimens increase with increasing TPU ratio and the specimens with series programmable filaments have higher strain to failure. The specimens with a 90° raster angle show the lowest strain to failure.

Overall, increasing the PLA contents can increase the strength and stiffness, while increasing TPU contents can increase the strain to failure of the printed objects. Varying arrangements and PLA:TPU compositions of programmable filaments and raster angles enable tuning the mechanical responses and properties of the printed objects between the extreme properties of the PLA and TPU specimens. The programmable filaments can create more complex failure paths in the dogbone specimens, hence extending the specimens' resistance to loads by extending failure strains as opposed to sudden breakage similar to in pure PLA specimens.

The corresponding MOE values of the mechanical properties of the dogbone specimens are given in Fig. A.10 in the Appendix. For most cases, the MOE values are below 10%, except for three cases, i.e., the MOE value of the elastic modulus of the 45° raster TPU dogbones is 17.2%, and the MOE values of the strain at failure, for 45° raster with parallel and series programmable filaments of PLA:TPU = 40:60 dogbones are approximately 14%. We are not sure about the lower reliability, or high variability in the data, for some of the mechanical properties of the dogbones with the 45° raster angle. To address the issue, more repeated tests are likely needed. The main purpose of this study is to examine the ability to tune the mechanical properties of the materials using programmable filaments, which has been demonstrated.

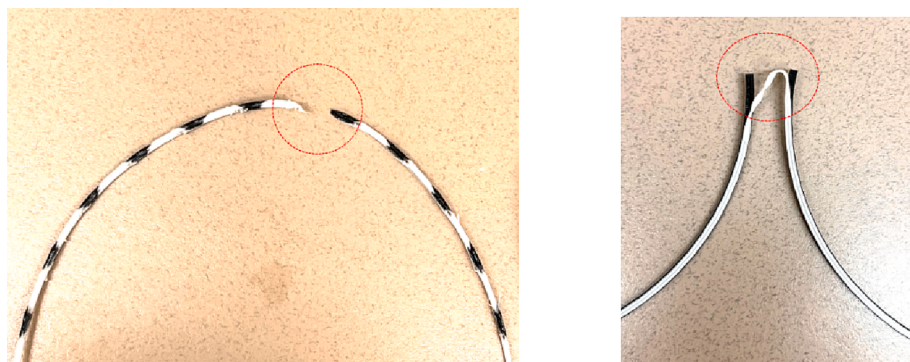
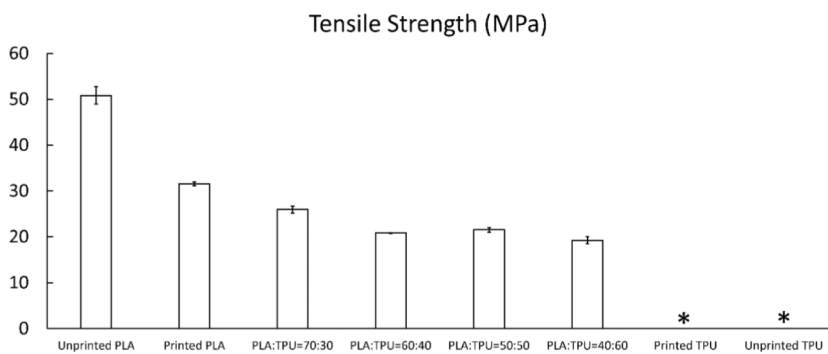
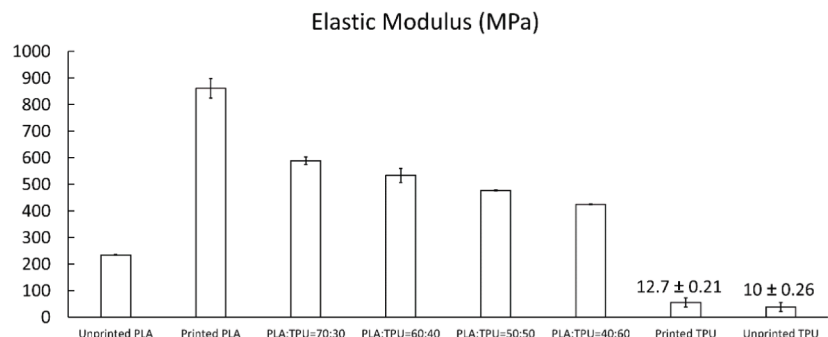
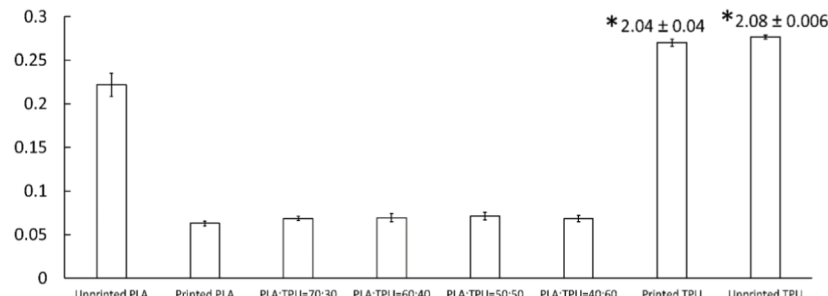


**Fig. 16.** Series (left) and parallel (right) configuration filaments after failure.



(\* The printed and unprinted TPU filament does not break therefore its tensile strength is not measured)

#### Strain at Failure



(The strain for printed and unprinted TPU filament is the last recorded strain for the tensile testing as it does not break)

**Fig. 17.** Average values with a standard deviation of Elastic Modulus (MPa), Tensile Strength (MPa), and Strain at Failure for all the parallel filaments.

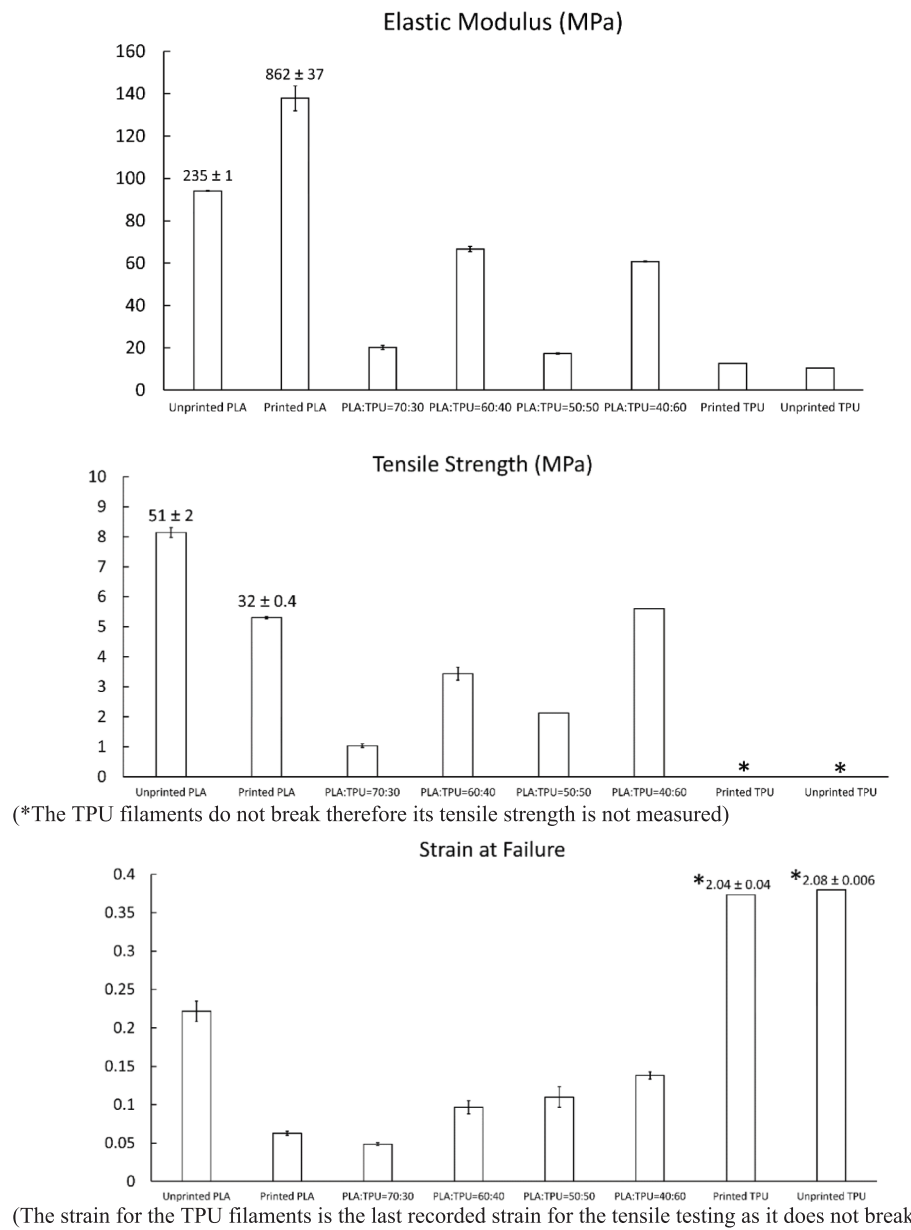


**Fig. 18.** Average values with a standard deviation of Elastic Modulus (MPa), Tensile Strength (MPa), and Strain at Failure for all the series filaments.

## 6. Discussion and conclusion

This study explores the possibility to tune mechanical behaviors and properties of 3D-printed objects by fabricating programmable filaments with controlled constituent compositions and arrangements. The study is designed based on the idea of combining two or more materials that differ significantly in their mechanical properties and with varying microstructural arrangements, we can acquire new properties between the extreme ends of their parent materials. Instead of blending multi-materials to create a new homogeneous blend through for example melt process like previously considered in the literature, in this study we also include the design of microstructural geometries that will contribute to controlling the overall mechanical responses of the printed object, particularly useful for low-cost, FDM 3D printing in a single extruder, using processing parameter adjustment. To demonstrate this idea, programmable filaments comprising stiff (brittle) PLA and soft (flexible) TPU with series and parallel arrangements have been considered. In this study, different volume ratios of PLA and TPU are studied to

generate new materials that are quite compliant (flexible) with relatively high strength. By printing with programmable filaments at different raster angles, we can further tune the mechanical behaviors and properties of the specimens.

When the thermoplastic PLA and TPU filaments undergo the printing process, the heating and cooling processes significantly change the mechanical response of PLA thermoplastic filament, see Fig. 13. As in the case of TPU filament, the printing process only slightly changes its mechanical responses. The printed filaments have a much smaller diameter than the original filaments (1.75 mm), indicating that shrinkage has occurred during printing (Fig. 7). The printing process altered the chemical and physical properties of the filaments, which can be attributed to a phase transformation during the heating and cooling processes. To be able to test printed PLA and TPU filaments, it is necessary to layer multiple extruded filaments and as a result, the printed filaments have non-negligible porosity compared to the unprinted filaments. In the case of PLA filaments, the densification in the printed filament may contribute to the significant increases in the

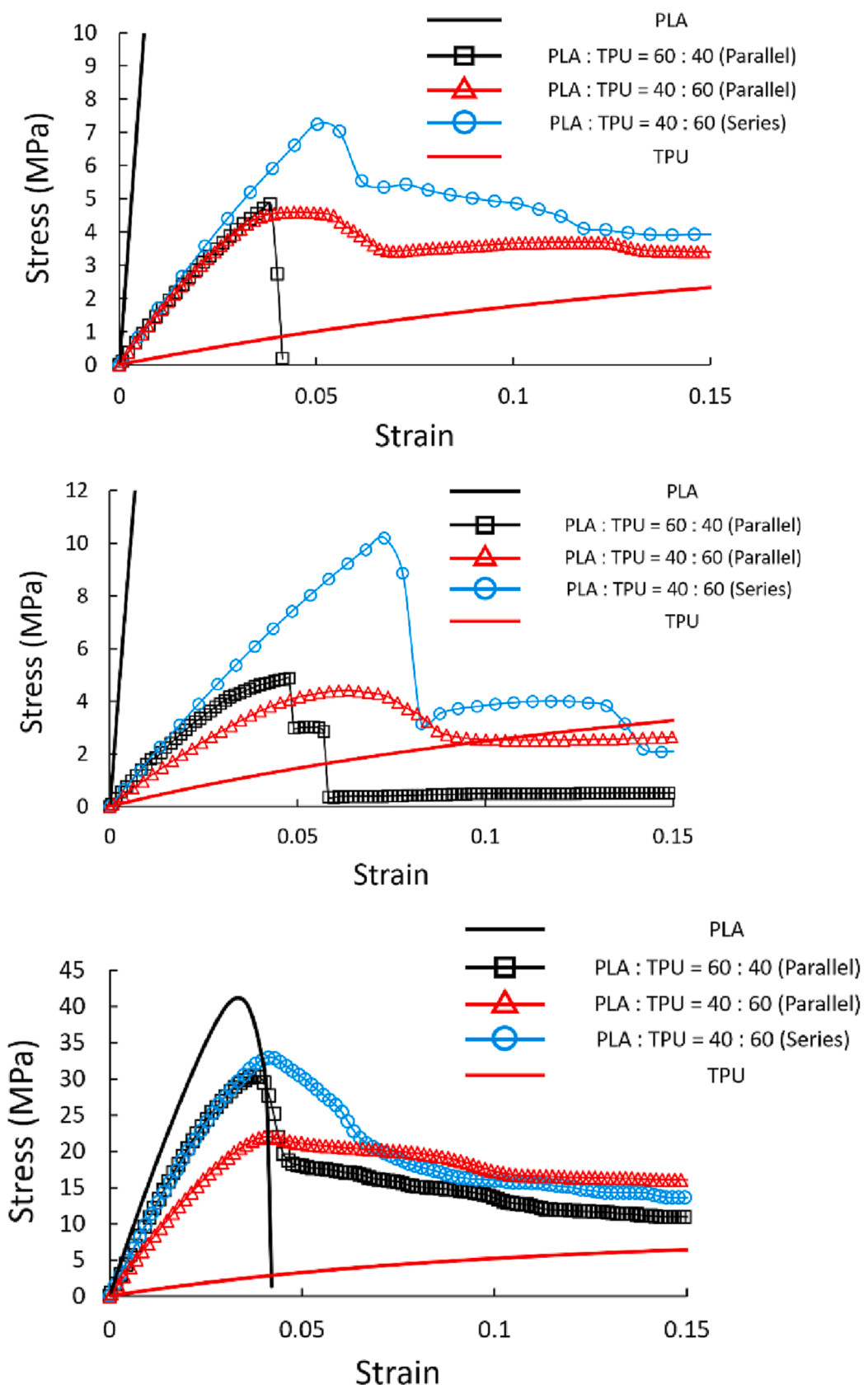


Fig. 19. Representative Stress-Strain curve for (top) 0° raster angle; (middle) 45° raster angle; (bottom) 90° raster angle dogbone specimens.



**Fig. 20.** 0°, 45°, 90° raster angle dogbone specimens ((a): PLA, (b): PLA:TPU = 60:40 in parallel, (c): PLA:TPU = 40:60 in parallel, (d): PLA:TPU = 40:60 in series, (e): TPU) after failure.

stiffness and the porosity reduces the strength. For the TPU, insignificant changes in the mechanical properties between the printed and unprinted filaments might be due to the stiffening from densification being offset by high porosity. Future studies can consider modeling the phase transformation during the printing process to explain how the mechanical properties of filaments change after printing.

From Figs. 14–16 (also Figs. A1–A2 and Tables A.1 and A.2), the programmable filaments have increased ductility and flexibility as compared to the PLA filament and decreased flexibility (stretch) and increased stiffness and strength as compared to the TPU filament. In the programmable filaments with a parallel arrangement increasing the PLA ratios results in stiffer and stronger filaments while no significant changes in the strain to failure are observed. In the parallel arrangement under uniaxial tension along the filament axis, the two filaments are subjected to the same displacement and that failure in one filament, i.e., PLA, limits further loading of the filament. When the PLA breaks, even though the TPU can still bear some load, the load-bearing ability and stiffness of the programmable filament reduce significantly. The programmable filament with a parallel arrangement of PLA and TPU has a larger contact area and relatively good bonding at the interface which delayed failures due to interfacial separation.

In the case of a series arrangement, the programmable filaments show lower average modulus and strength compared to the parallel configuration filaments. This can be attributed to the fact that the series

configuration has a lower contact (interfacial) the area between the PLA and TPU materials than the parallel configuration and possibly a rather weak interfacial bonding and thus, early failure due to an interfacial separation is seen with relatively low ultimate stress. A higher percentage of TPU leads to a higher length of TPU segments in the series programmable filament and hence leads to higher failure strain. In the future, we will need to investigate an approach to improve bonding between the PLA and TPU in a series manner so we can generate a programmable filament with more flexible behaviors and enhanced strength.

The arrangements of the constituent materials (PLA and TPU) in the programmable filaments influence the mechanical behaviors and properties of dogbone specimens. While the programmable filament with the series arrangement of PLA and TPU shows weaker strength and stiffness compared to the one with parallel arrangement due to the weaker bond strength under uniaxial tension, the dogbone specimens printed with the series arrangement of programmable filaments show higher tensile modulus and strength when compared to the ones of the parallel arrangement programmable filaments (see Figs. 19, 21–23 and Tables A.3–A.5).

In both arrangements, alternating patterns of PLA and TPU are seen (as illustrated in Fig. 24). This pattern of stiff (and strong) and soft constituents can delay failure and enhance load-bearing ability due to an increase in internal energy needed to induce deformation in this arrangement, i.e., when the brittle constituent breaks due to a low strain resistant the adjacent soft constituent can still hold the system together and transfer the load to the stronger constituent. The series arrangement of the programmable filament creates some portion of interlocking microstructures of PLA and TPU of the dogbones, which explains the higher stiffness and strength in the dogbone specimens printed with the series arrangements of PLA:TPU programmable filaments. It is noted that even when the dogbone specimens with series programmable filaments have a lower ratio of PLA, i.e., PLA:TPU = 40:60, their stiffness and strength are still higher than the specimens printed with parallel programmable filaments with PLA:TPU = 60:40, which might be attributed to the interlocking microstructures in the dogbone specimen.

In addition to varying the arrangement of PLA and TPU in the filaments, changing the raster angle that impacts the mechanical responses of the composites and alters the failure behaviors. For the 90° raster angle specimens, the microstructural arrangements with regards to the loading direction lead to complex failure patterns (see Fig. 20) as the flexible and compliant TPU prevents immediate specimen breakages and continues transferring loads to the undamaged region in the specimens, which results in high modulus and tensile strength amongst all the other raster angle specimens. For the 0° raster angle dogbone specimens, the layers fail due to separation between printed layers, which explains the nearly similar moduli and strength of all dogbone specimens with different programmable filaments. The specimens with 0° raster angle show the lowest moduli and strength. The 45° raster angle specimens experience both shear and tensile behavior characteristics.

From limited statistical analysis, i.e., average, standard deviation, and MOE, we conclude that most of the tested data indicate a higher reliability of the experimental data and that it can confidently represent the population of the specimens. A few data, i.e., the strain at failure for the PLA:TPU = 50:50 filament, modulus of TPU dogbones with 45° raster, and strain at failure of dogbones with 45° raster out of series and parallel programmable filaments of 40:60 PLA:TPU, shows larger variability (MOE values are between 10 and 20%). Further study can consider a larger number of samples to perform a more robust statistical analysis.

Overall, we demonstrate that new mechanical properties and responses of materials can be achieved using low-cost FDM printing by altering the constituent compositions, microstructural arrangements,

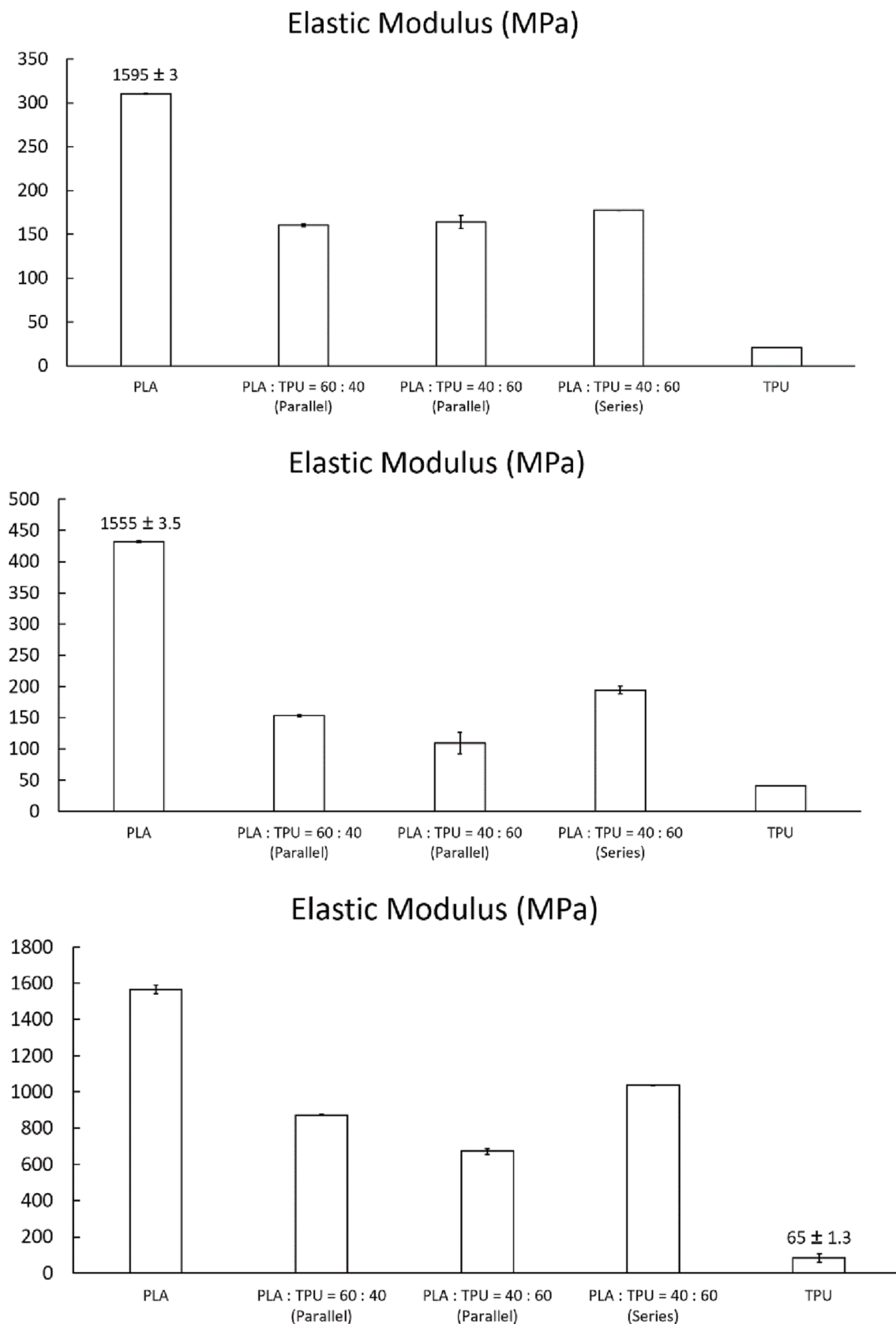


Fig. 21. Elastic Modulus (MPa) of dogbone specimens with raster angles 0° (top), 45° (middle), and 90° (bottom).

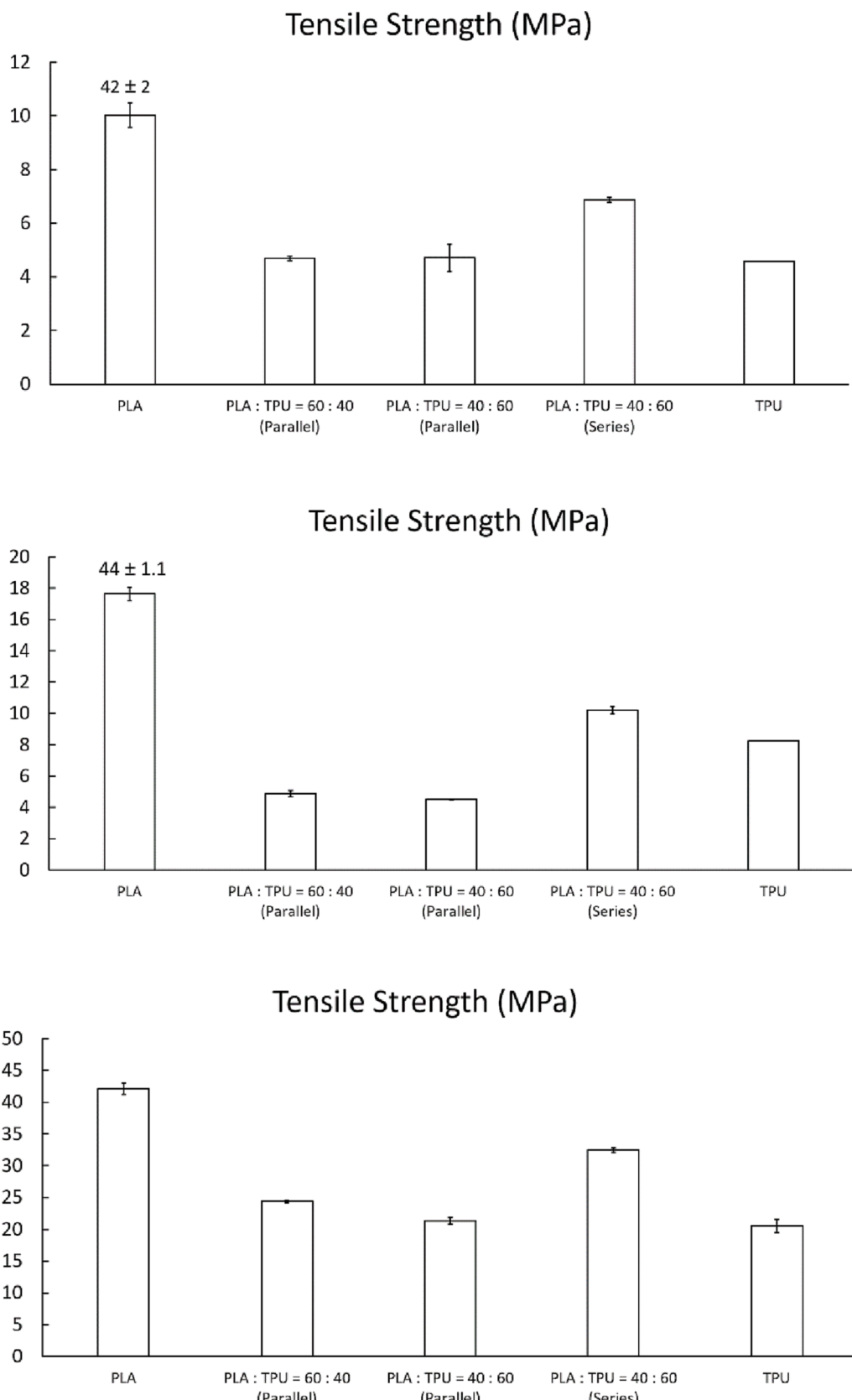
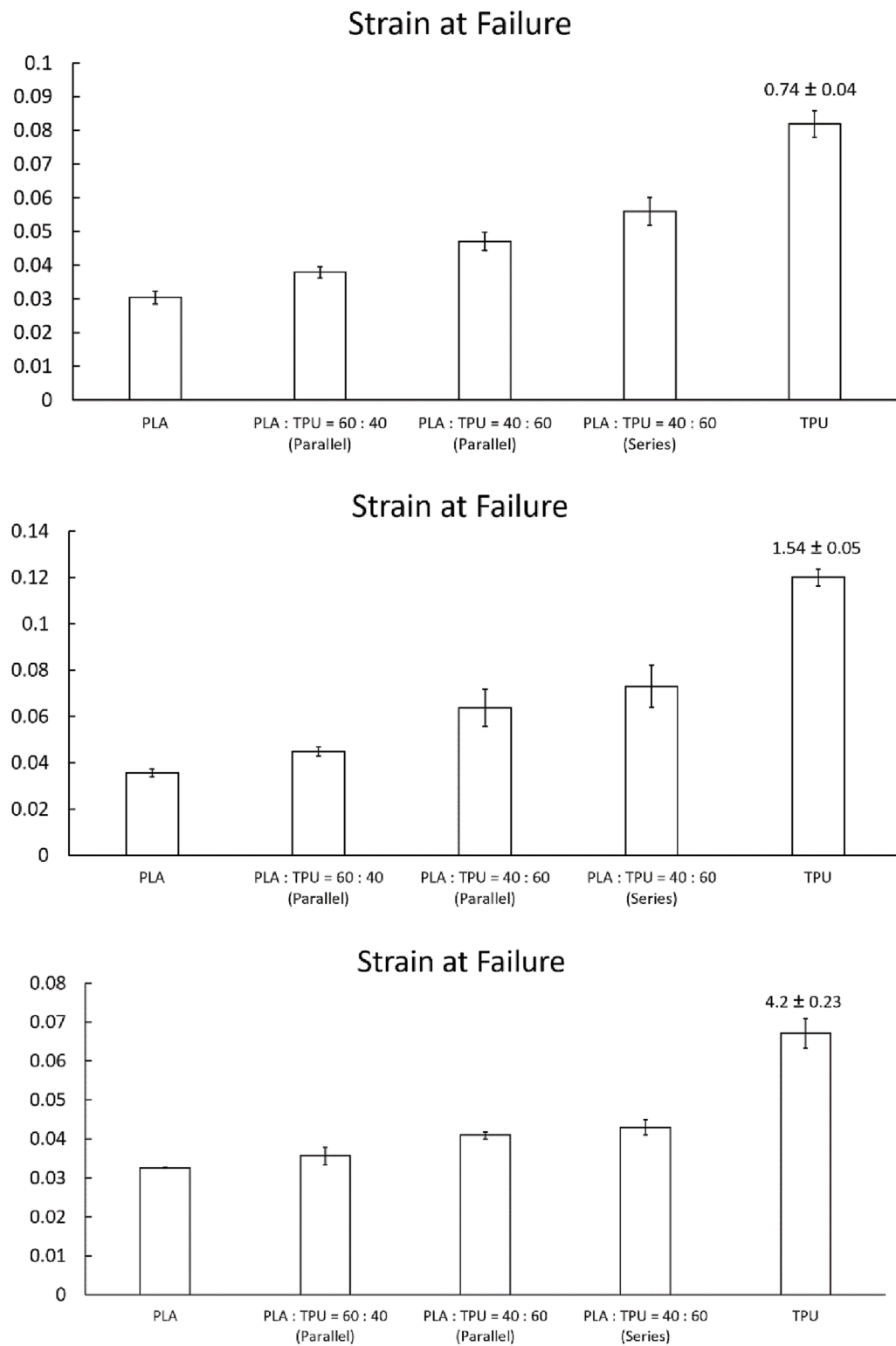
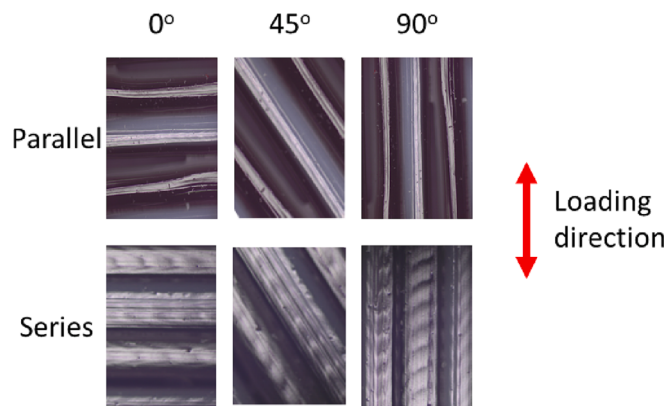


Fig. 22. Tensile Strength (MPa) of dogbone specimens with raster angles 0° (top), 45° (middle), and 90° (bottom).



**Fig. 23.** Strain at Failure of dogbone specimens with raster angles 0° (top), 45° (middle), and 90° (bottom).



**Fig. 24.** Arrangement of PLA and TPU in the dogbone specimen printed with programmable filaments of parallel configuration (top) and series configuration (bottom).

and raster angles during printing. Future work can consider alternating raster angles in each layer to increase the bonding of layers and thus strength in 3D printed objects, investigating other printing parameters that significantly affected the mechanical responses (e.g., nozzle speed, printing temperature, and the gap between the nozzle and room temperature) of the 3D printed object using programmable filaments, as well as modeling the mechanical performance of the programmable filaments and dogbone specimens. This will enable systematically tuning the mechanical properties of the printed parts and minimize extensive experiments to explore new material properties in multi-material printing.

## Declaration of Competing Interest

The authors declare that they have no known competing financial interests or personal relationships that could have appeared to influence the work reported in this paper.

## Data availability

Data will be made available on request.

## Acknowledgment

This work is supported by the National Science Foundation under grant CMMI 2222935.

## Data Availability

The raw data required to reproduce these findings will be made available when the manuscript is accepted.

## Appendix A

This section summarizes results from uniaxial tensile tests of programmable filaments with series and parallel arrangements from three different repeated tests (Figs. A1-A2). The slight variabilities in the test results can be attributed to the heterogeneity of the filaments, and measurement variations (both human and machine) throughout the testing procedure. Tables A1 and A2 summarized the mechanical properties of the programmable filaments.

The uniaxial tensile testing results of dogbone specimens printed with different raster angles from various PLA, TPU, and programmable filaments are summarized in Figs. A5-A9. The mechanical properties of the dogbone specimens are summarized in Tables A.3-A.5.

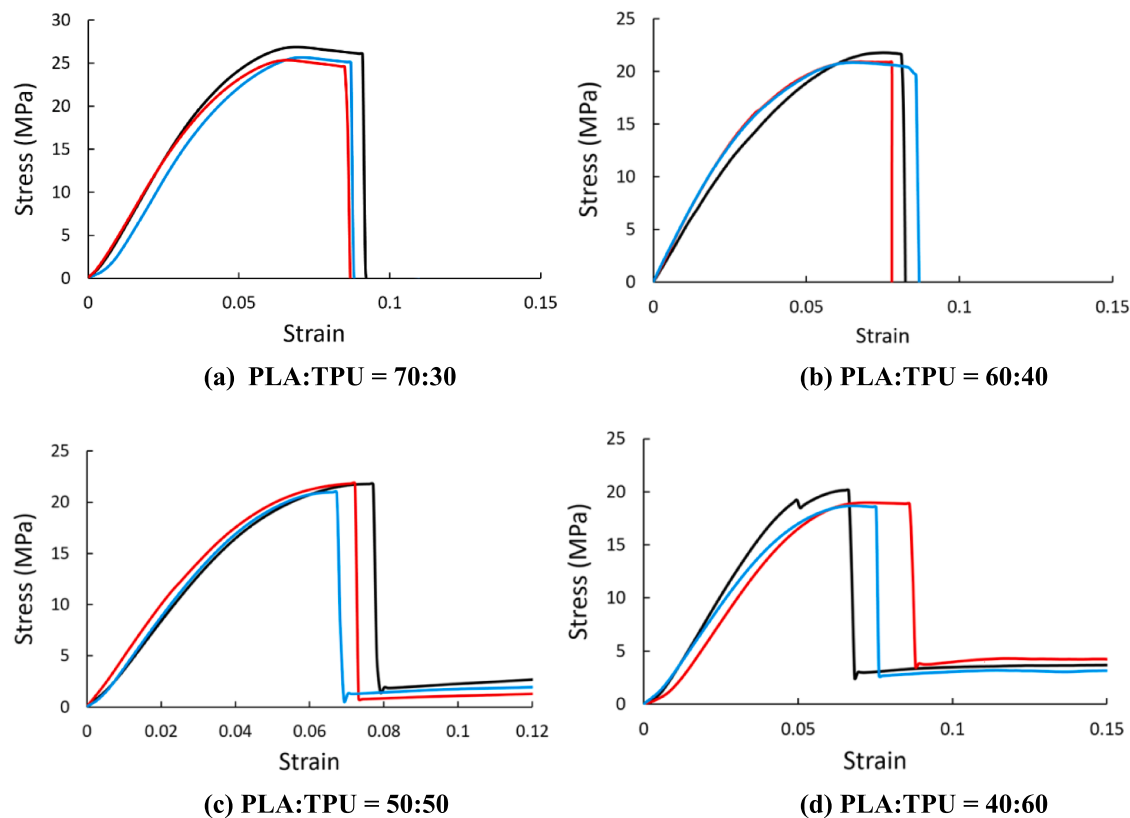


**Fig. A1.** Stress-Strain curves for parallel configuration programmable filaments with different ratios of PLA:TPU.

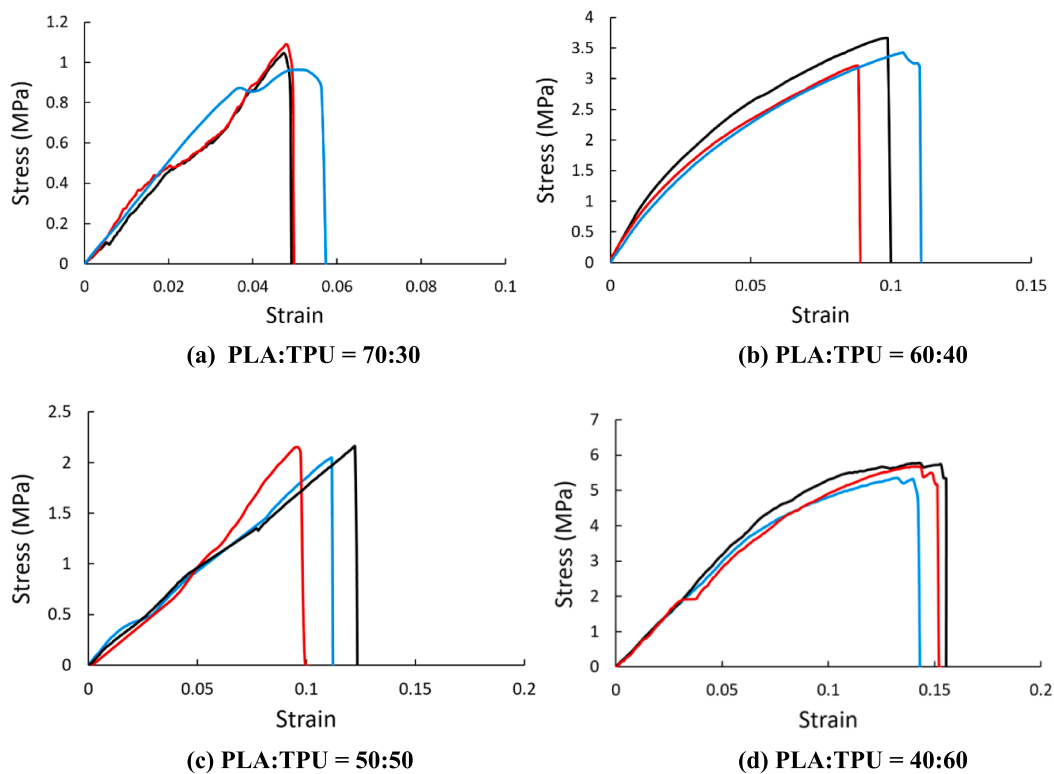
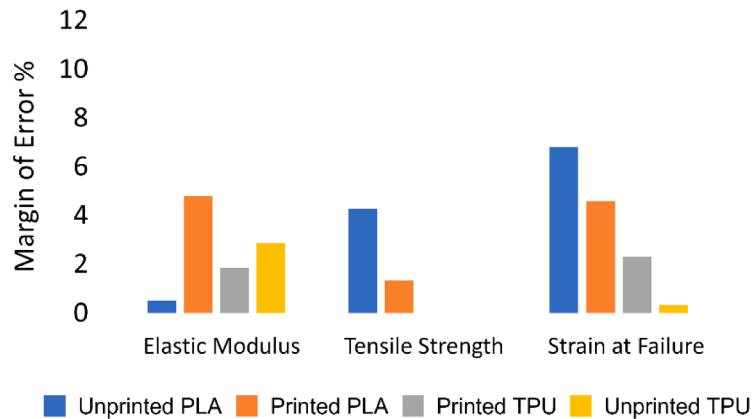


**Fig. A2.** Stress-Strain curves for series configuration programmable filaments with different ratios of PLA:TPU.



\*TPU filaments do not break

**Fig. A3.** Margin of Error % for unprinted and printed PLA and TPU filaments.

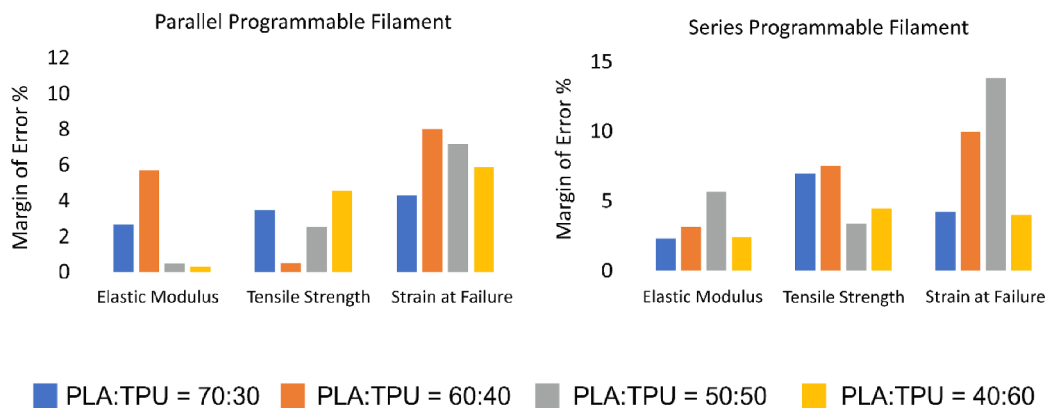


**Fig. A4.** Margin of Error % for programmable parallel (left) and series (right) filaments.

**Table A1**

Mechanical Properties (Elastic Modulus, Tensile Strength, and Strain at failure) of the programmable filaments with a parallel arrangement.

Material(s)	E (MPa)	$\sigma$ (MPa)	$\epsilon_f$
	Avg. $\pm$ S.D.	Avg. $\pm$ S.D.	Avg. $\pm$ S.D.
Unprinted PLA	234.72 $\pm$ 1.05	50.86 $\pm$ 1.92	0.22 $\pm$ 0.013
Printed PLA	861.88 $\pm$ 36.61	31.57 $\pm$ 0.38	0.063 $\pm$ 0.002
PLA:TPU = 70:30	589.38 $\pm$ 13.90	25.96 $\pm$ 0.80	0.068 $\pm$ 0.0026
PLA:TPU = 60:40	533.95 $\pm$ 26.88	20.84 $\pm$ 0.09	0.069 $\pm$ 0.0049
PLA:TPU = 50:50	477.44 $\pm$ 2.01	21.53 $\pm$ 0.48	0.071 $\pm$ 0.0045
PLA:TPU = 40:60	425.42 $\pm$ 1.22	19.27 $\pm$ 0.78	0.068 $\pm$ 0.0035
Printed TPU	12.73 $\pm$ 0.21	N/A *	2.04 $\pm$ 0.04*
Unprinted TPU	10.44 $\pm$ 0.26	N/A *	2.08 $\pm$ 0.006*

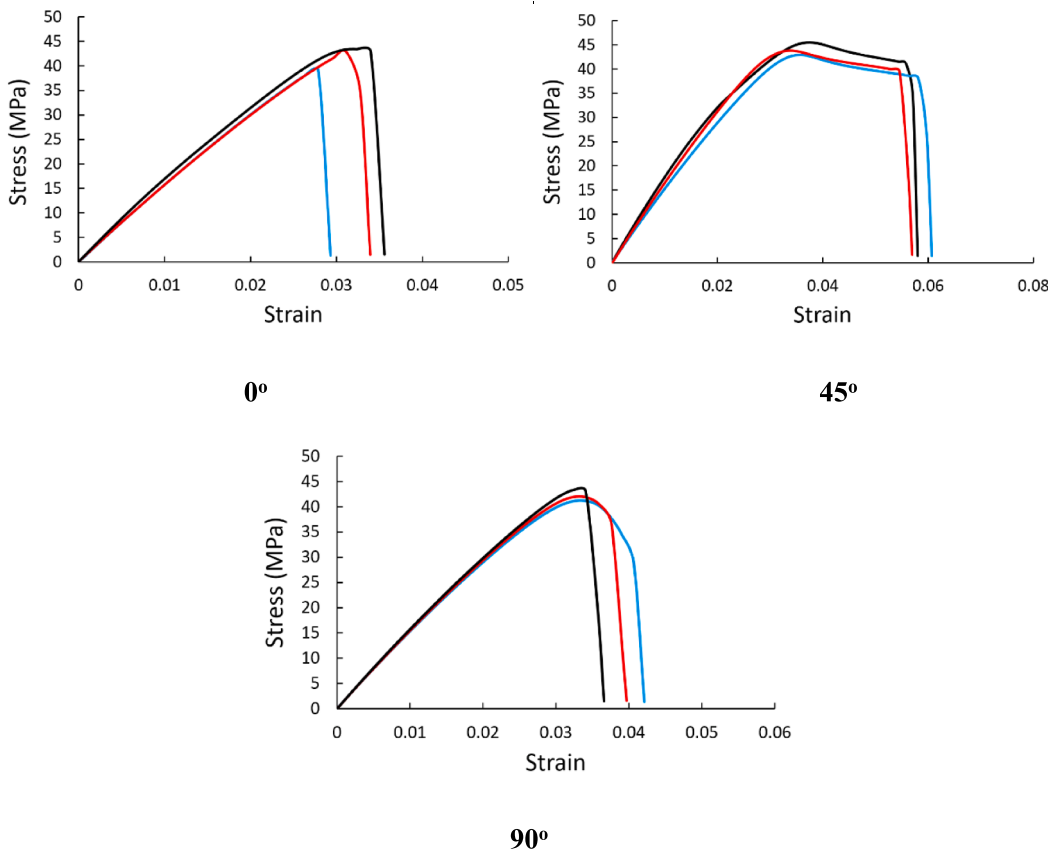
\*TPU filament did not break and strain 2.09 is the final recorded strain.

**Table A2**

Mechanical Properties (Elastic Modulus, Tensile Strength, and Strain at failure) of the programmable filaments with a series arrangement.

Material(s)	E (MPa)	$\sigma$ (MPa)	$\epsilon_f$
	Avg. $\pm$ S.D.	Avg. $\pm$ S.D.	Avg. $\pm$ S.D.
Unprinted PLA	234.72 $\pm$ 1.05	50.86 $\pm$ 1.92	0.22 $\pm$ 0.013
Printed PLA	861.88 $\pm$ 36.61	31.57 $\pm$ 0.38	0.063 $\pm$ 0.002
PLA:TPU = 70:30	20.23 $\pm$ 0.41	1.03 $\pm$ 0.06	0.047 $\pm$ 0.0018
PLA:TPU = 60:40	66.69 $\pm$ 1.87	3.43 $\pm$ 0.23	0.096 $\pm$ 0.0085
PLA:TPU = 50:50	17.36 $\pm$ 0.87	2.12 $\pm$ 0.06	0.11 $\pm$ 0.013
PLA:TPU = 40:60	60.81 $\pm$ 1.30	5.60 $\pm$ 0.22	0.14 $\pm$ 0.005
Printed TPU	12.73 $\pm$ 0.21	N/A *	2.04 $\pm$ 0.04*
Unprinted TPU	10.44 $\pm$ 0.26	N/A *	2.08 $\pm$ 0.006*

\*TPU filament did not break and strain 2.09 is the final recorded strain.

**Fig. A5.** Stress – Strain curves for 0°, 45° and 90° degree raster angle dogbones printed using pure PLA filament.

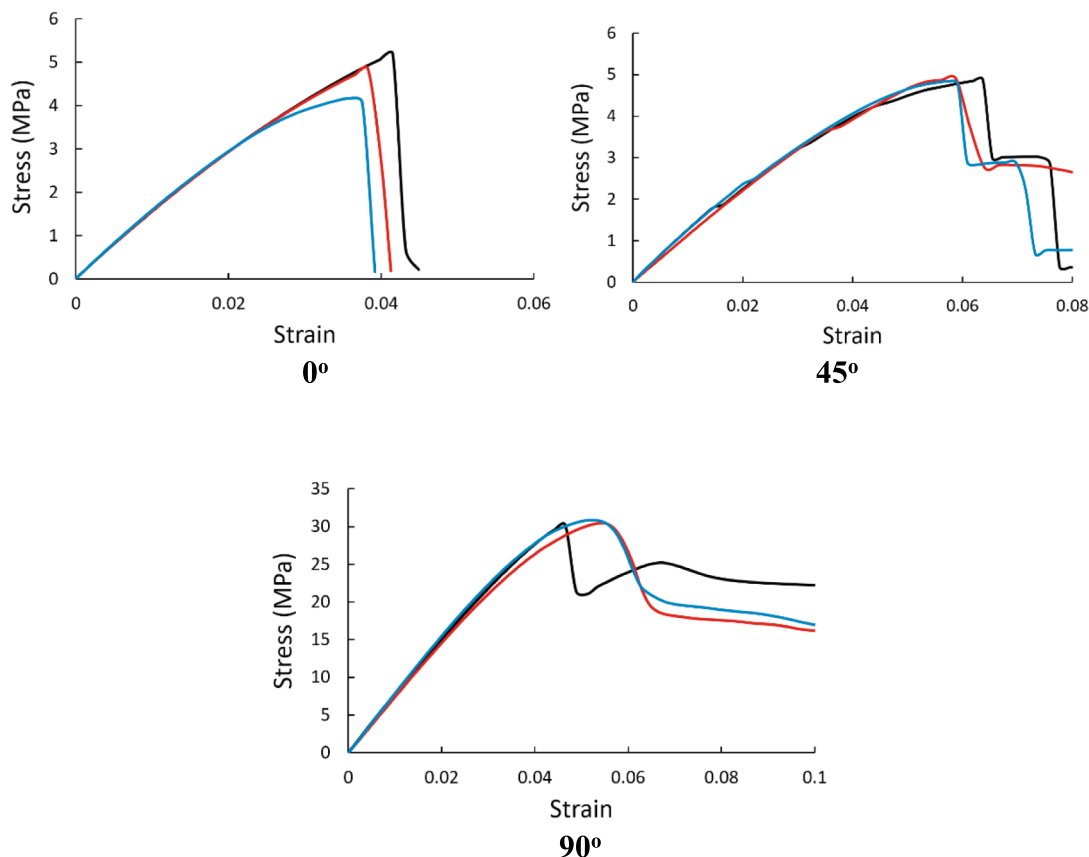


**Fig. A6.** Stress-Strain curves for 0°, 45°, and 90° degree raster angle printed dogbones using parallel configuration PLA:TPU 60:40 programmable filament.

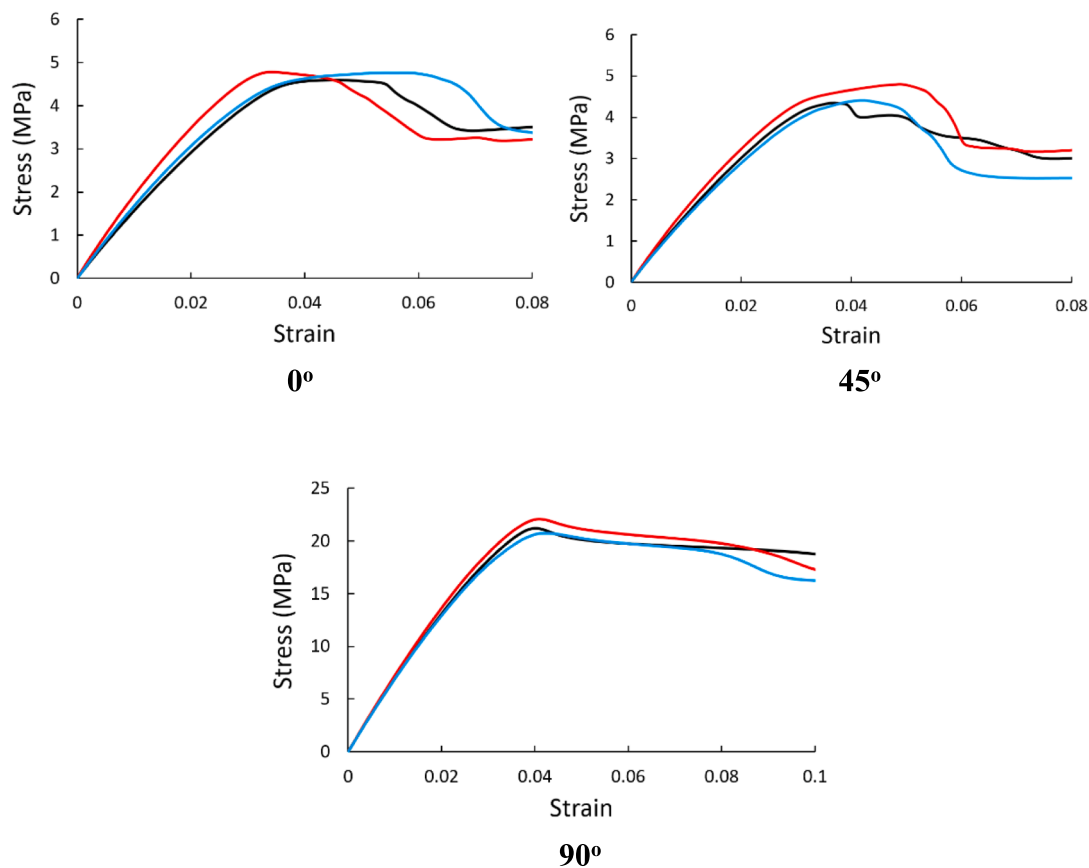


**Fig. A7.** Stress-Strain curves for 0°, 45°, and 90° degree raster angle printed dogbones using parallel configuration PLA:TPU 40:60 programmable filament.

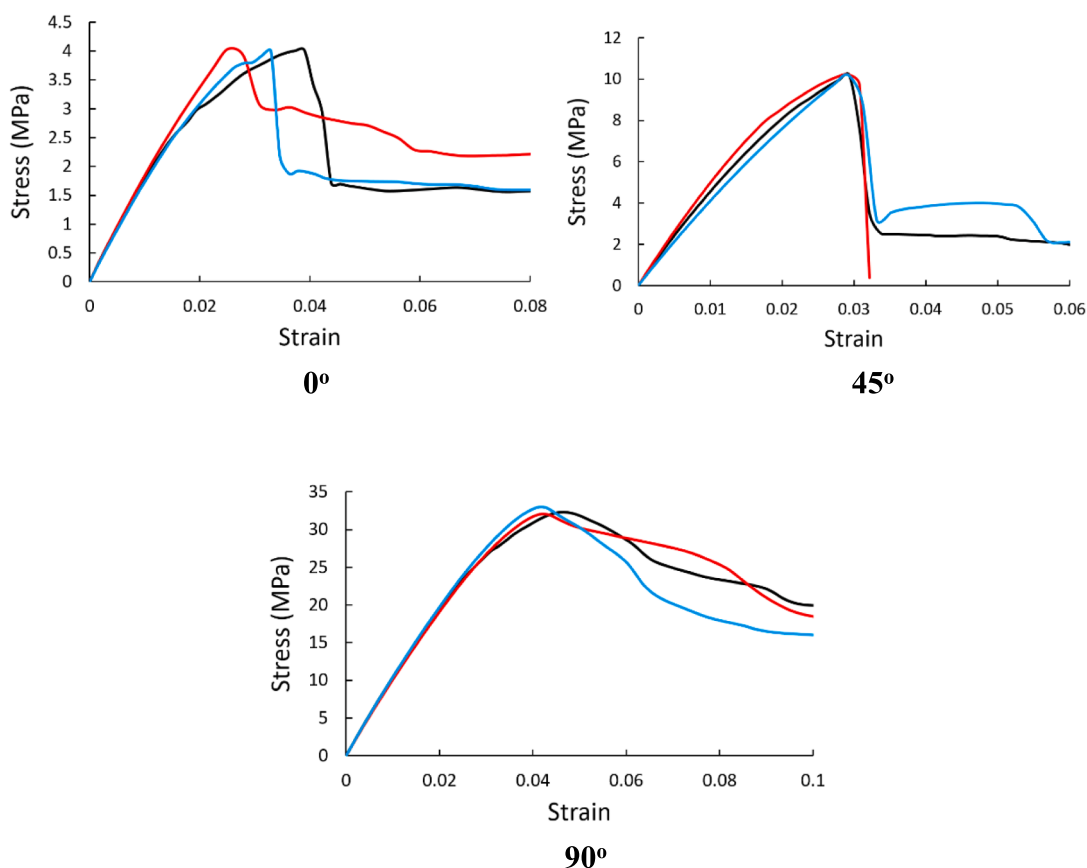


**Fig. A8.** Stress-Strain curves for 0°, 45°, and 90° degree raster angle dogbones printed using series configuration PLA:TPU 40:60 programmable filament.

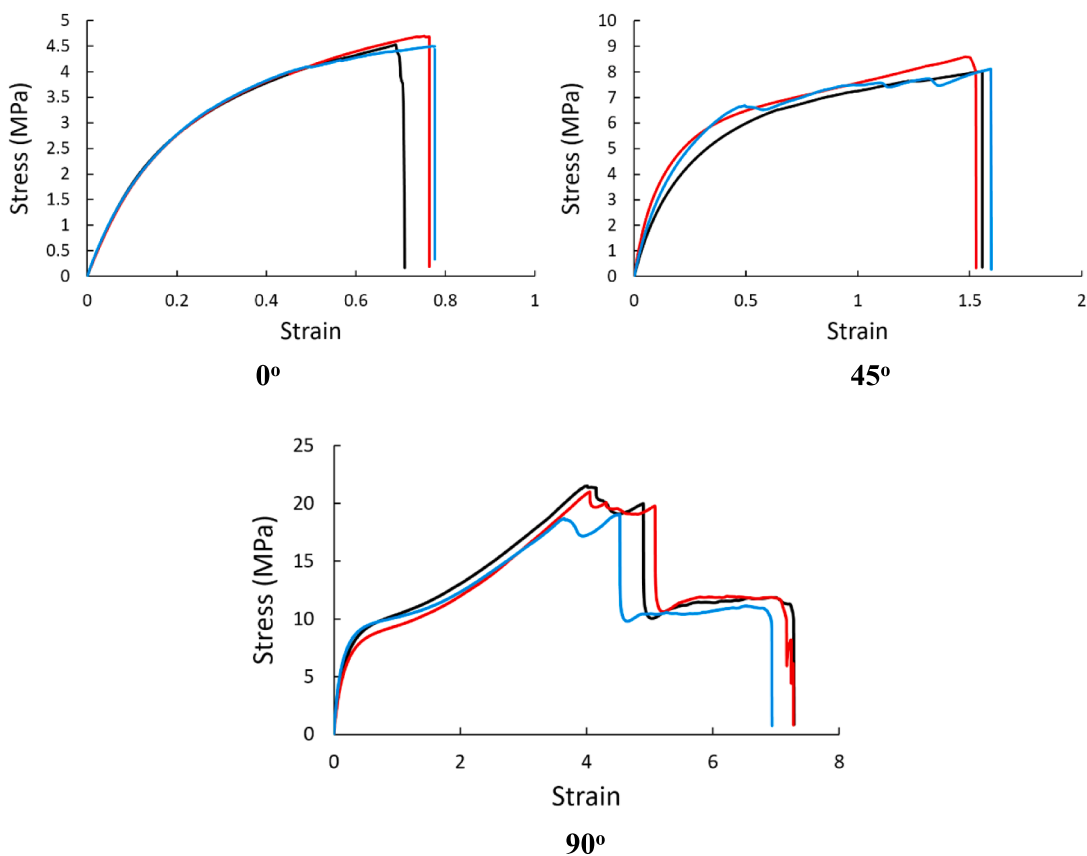


**Fig. A9.** Stress – Strain curves for 0°, 45° and 90° degree raster angle printed using pure TPU filament.

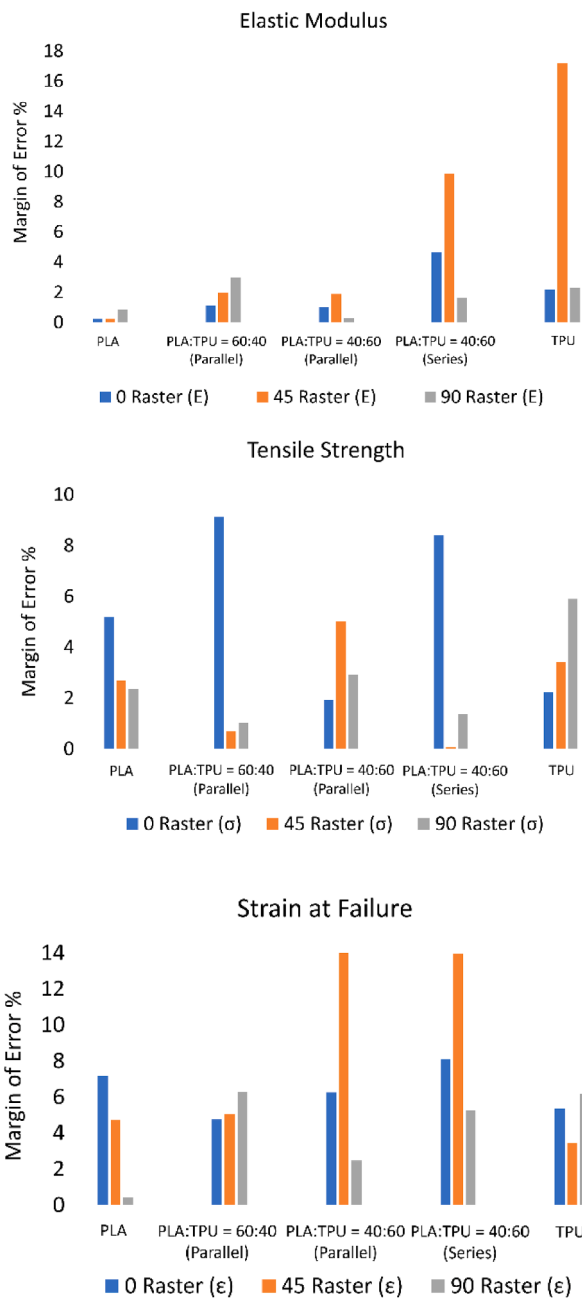


**Fig. A10.** Margin of Error % for programmable parallel (left) and series (right) filaments.

**Table A3**

Mechanical Properties (Elastic Modulus, Tensile Strength, and Strain at failure) of the tested specimens for 0° Raster Angle.

Type	Material(s)	E (MPa)		
		Avg. ± S.D.	σ (MPa)	ε <sub>f</sub>
-	PLA	1595.06 ± 3.00	41.78 ± 1.91	0.030 ± 0.0019
Parallel	PLA:TPU 60:40	160.40 ± 1.58	4.70 ± 0.38	0.038 ± 0.0016
Parallel	PLA:TPU 40:60	164.01 ± 1.47	4.71 ± 0.08	0.047 ± 0.0026
Series	PLA:TPU 40:60	177.54 ± 7.32	6.86 ± 0.51	0.056 ± 0.004
-	TPU	20.68 ± 0.40	4.57 ± 0.09	0.74 ± 0.035

**Table A4**

Mechanical Properties (Elastic Modulus, Tensile Strength, and Strain at failure) of the tested specimens for 45° Raster Angle.

Type	Material(s)	E (MPa)		
		Avg. ± S.D.	σ (MPa)	ε <sub>f</sub>
-	PLA	1554.61 ± 3.47	44.04 ± 1.05	0.036 ± 0.0015
Parallel	PLA:TPU 60:40	153.45 ± 2.70	4.87 ± 0.03	0.045 ± 0.002
Parallel	PLA:TPU 40:60	109.23 ± 1.82	4.52 ± 0.20	0.064 ± 0.008
Series	PLA:TPU 40:60	194.56 ± 16.98	10.2 ± 0.006	0.073 ± 0.009
-	TPU	41.34 ± 6.28	8.24 ± 0.25	1.54 ± 0.047

**Table A5**

Mechanical Properties (Elastic Modulus, Tensile Strength, and Strain at failure) of the tested specimens for 90° Raster Angle.

Type	Material(s)	E (MPa)		
		Avg. ± S.D.	σ (MPa)	ε <sub>f</sub>
-	PLA	1565.12 ± 11.72	42.14 ± 0.88	0.033 ± 0.00013
Parallel	PLA:TPU 60:40	873.52 ± 23.02	24.38 ± 0.22	0.036 ± 0.002
		672.33 ± 1.66	21.32 ± 0.55	0.041 ± 0.0009
Series	PLA:TPU 40:60	1036.09 ± 15.01	32.45 ± 0.39	0.043 ± 0.002
		64.92 ± 1.32	20.52 ± 1.07	4.20 ± 0.23

## References

- [1] Hamzah HH, et al. 3D printable conductive materials for the fabrication of electrochemical sensors: A mini review. *Electrochim Commun* 2018;96:27–31.
- [2] Zheng Y, et al. Scientometric analysis and systematic review of multi-material additive manufacturing of polymers. *Polymers* 2021;13(12):1957.
- [3] Vaezi M, et al. Multiple material additive manufacturing—Part 1: a review: this review paper covers a decade of research on multiple material additive manufacturing technologies which can produce complex geometry parts with different materials. *Virtual and Physical Prototyping* 2013;8(1):19–50.
- [4] Bandyopadhyay A, Heer B. Additive manufacturing of multi-material structures. *Mater Sci Eng R Rep* 2018;129:1–16.
- [5] Rafiee M, Farahani RD, Therriault D. Multi-material 3D and 4D printing: a survey. *Adv Sci* 2020;7(12):1902307.
- [6] Khondoker MAH, Asad A, Sameoto D. Printing with mechanically interlocked extrudates using a custom bi-extruder for fused deposition modelling. *Rapid Prototyp J* 2018.
- [7] Wang X, et al. 3D printing of polymer matrix composites: A review and prospective. *Compos B Eng* 2017;110:442–58.
- [8] Skylar-Scott MA, et al. Voxulated soft matter via multimaterial multinozzle 3D printing. *Nature* 2019;575(7782):330–5.
- [9] Han D, Lee H. Recent advances in multi-material additive manufacturing: Methods and applications. *Curr Opin Chem Eng* 2020;28:158–66.
- [10] Espalin D, et al. Multi-material, multi-technology FDM: exploring build process variations. *Rapid Prototyp J* 2014.
- [11] Cecil F, et al. One step multi-material 3D printing for the fabrication of a photometric detector flow cell. *Anal Chim Acta* 2020;1097:127–34.
- [12] Tao Y, et al. Application of a thermoplastic polyurethane/poly(lactic acid) composite filament for 3D-printed personalized orthosis. *Mater Technol* 2019;53:71–6.
- [13] Hart KR, Dunn RM, Wetzel ED. Tough, Additively Manufactured Structures Fabricated with Dual-Thermoplastic Filaments. *Adv Eng Mater* 2020;22(4):1901184.
- [14] Loke G, et al. Structured multimaterial filaments for 3D printing of optoelectronics. *Nat Commun* 2019;10(1):1–10.
- [15] Kalita SJ, et al. Development of controlled porosity polymer-ceramic composite scaffolds via fused deposition modeling. *Mater Sci Eng C* 2003;23(5):611–20.
- [16] Zhou Z, et al. Development of a direct feed fused deposition modelling technology for multi-material manufacturing. In: AIP Conference Proceedings. 20AIP Publishing.
- [17] Kwon N, et al. Multi-ttach: Techniques to Enhance Multi-material Attachments in Low-cost FDM 3D Printing. In: Symposium on Computational Fabrication; 2021.
- [18] Takahashi H, Punpongsan P, Kim J. Programmable filament: Printed filaments for multi-material 3D printing. In: Proceedings of the 33rd Annual ACM Symposium on User Interface Software and Technology; 2020.

- [19] Oksiuta Z, et al. Mechanical and Thermal Properties of Polylactide (PLA) Composites Modified with Mg, Fe, and Polyethylene (PE) Additives. *Polymers* 2020;12(12):2939.
- [20] Jaso V, et al. Bio-plastics and elastomers from polylactic acid/thermoplastic polyurethane blends. *J Appl Polym Sci* 2014;131(22).
- [21] Hong H, et al. A novel composite coupled hardness with flexibility—polylactic acid toughen with thermoplastic polyurethane. *J Appl Polym Sci* 2011;121(2):855–61.
- [22] Zhao X, et al. Structure and blood compatibility of highly oriented poly (lactic acid)/thermoplastic polyurethane blends produced by solid hot stretching. *Polym Adv Technol* 2013;24(9):853–60.
- [23] Han JJ, Huang HX. Preparation and characterization of biodegradable polylactide/thermoplastic polyurethane elastomer blends. *J Appl Polym Sci* 2011;120(6):3217–23.
- [24] Spoerl M, et al. Effect of the printing bed temperature on the adhesion of parts produced by fused filament fabrication. *Plast, Rubber Compos* 2018;47(1):17–24.
- [25] ASTM D638-14. Standard Test Method for Tensile Properties of Plastics. ASTM International; 2014.
- [26] Kar Sing L, et al. Mechanical properties characterization and finite element analysis of epoxy grouts in repairing damaged pipeline. *J Press Vessel Technol* 2018;140(6).
- [27] Özen A, et al. Exploring the role of manufacturing parameters on microstructure and mechanical properties in fused deposition modeling (FDM) using PETG. *Appl Compos Mater* 2021;28(6):1799–828.
- [28] Pathan M, et al. Predictions of the mechanical properties of unidirectional fibre composites by supervised machine learning. *Sci Rep* 2019;9(1):1–10.
- [29] Fadiel AA, et al. A Comprehensive Evaluation of the Mechanical Properties of Rubberized Concrete. *J Compos Sci* 2023;7(3):129.
- [30] Akbari MK, et al. Al-TiB<sub>2</sub> micro/nanocomposites: Particle capture investigations, strengthening mechanisms and mathematical modelling of mechanical properties. *Mater Sci Eng A* 2017;682:98–106.